Continental Shelf Research 148 (2017) 89–103

Contents lists available at ScienceDirect

Continental Shelf Research

journal homepage: www.elsevier.com/locate/csr

Controlling factors of the seasonal variability of productivity in the southern Humboldt Current System (30–40°S): A biophysical modeling approach

Odette A. Vergara[a,b], Vincent Echevín[c], Héctor Hito Sepúlveda[d], Renato A. Quiñones[a,b,*]

[a] Interdisciplinary Center for Aquaculture Research, Universidad de Concepción, O´Higgins 1695, Concepción, Chile
[b] Doctorate Program in Oceanography, Department of Oceanography, Universidad de Concepción, Casilla 160-C, Concepción, Chile
[c] Laboratoire d' Oceanographie et de Climatologie: Expérimentation et Analyse Numérique (LOCEAN), Institute Pierre-Simon Laplace (IPSL), UPMC/CNRS/IRD/MNHN, 4 Place Jussieu, Case 100, 75252 Paris cedex 05, France
[d] Geophysics Department, University of Concepción, Concepción, Chile

ARTICLE INFO

Keywords:
Biogeochemical model
Humboldt Current System
Co-limitation of nutrients
Nutrient budget
ROMS-PISCES Model
Upwelling

ABSTRACT

The spatial and seasonal variability of nutrients and chlorophyll in the southern Humboldt Current System were assessed using a high-resolution regional ocean circulation model (ROMS) coupled to a biogeochemical model (Pelagic-Interactions Scheme for carbon and Ecosystem Studies; PISCES). The simulated nutrients and chlorophyll fields were validated using satellite and *in situ* observations at a continental shelf time-series station. The annual cycles of modeled chlorophyll and nutrients were consistent with the highest values observed in spring and summer, which is in agreement with enhanced upwelling observations. Co-limitation of phytoplankton growth by nutrients and light was analyzed for diatoms, the dominant phytoplankton group in the simulations. The results showed that co-limitation, near the coast, was governed in autumn and winter by light, and by silicate in spring and summer, whereas other nutrients were limiting offshore between January and April. Nutrient transport in the surface layer was analyzed. Vertical advection reflected areas with higher coastal upwelling, and was partly offset by horizontal processes related to eddy-induced transport from the nearshore to the open ocean. Vertical mixing was shown to play a key role in replenishing the surface layer with nutrients.

1. Introduction

Phytoplankton photosynthesis plays a key role in ocean biogeochemical cycles. It is the basis of marine trophic webs (Falkowski et al., 1998) and contributes to carbon sequestering and exportation as organic matter (Eppley and Peterson, 1979). Phytoplankton growth in the ocean requires optimal light conditions (Peterson et al., 1987), nutrient availability in the euphotic zone (Diehl et al., 2002) and adequate temperature (Nicklisch et al., 2008; Thomas et al., 2012). Nutrient concentrations increase with depth (Zehr and Ward, 2002), however, nutrient input in the well-lit surface layer can be stimulated by physical mechanisms such as coastal upwelling (Chávez et al., 2003), a major process in Eastern Boundary Upwelling Systems (EBUS). These regions are characterized by intense seasonally modulated upwelling events driven by alongshore winds. These winds force offshore surface Ekman horizontal flow, which is compensated by an upward flow of cool and nutrient-rich waters (Chávez and Messié, 2009), a well-described process known as coastal upwelling (e.g. Bakun, 1996; Hill et al., 1998).

The Humboldt Current System (HCS) off the coast of Chile is highly productive with primary production rates exceeding 25.8 g C m^{-2} d^{-1} (Montero et al., 2007; Quiñones et al., 2010). Here, upwelling is driven when S-SW winds (i.e. equatorward) blow with moderate to high intensity (> 5 ms^{-1}) (Marín et al., 2003) in summer, bringing Equatorial Subsurface Water (ESSW) to the surface. This water mass is associated with low concentrations of dissolved oxygen (< 0.5 mL L^{-1}), high salinity, low temperature (Atkinson et al., 2002; Strub et al., 1998; Sobarzo et al., 2007) and high concentrations of inorganic nutrients (Silva et al., 2009).

In addition to upwelling, other regulating factors of primary productivity determine the spatial and temporal distribution of phytoplankton biomass. One is vertical mixing, which determines the mixed layer depth that can vary from a few meters to more than 100 m (Kirk, 1994). Variations in mixed layer depth affect phytoplankton dynamics by controlling nutrient and light availability (Sverdrup, 1953). Echevin et al. (2008) used model simulations to show that wind-driven seasonal upwelling (i.e. vertical flux of nutrients to the surface layer) in the Peruvian EBUS was not a controlling factor of seasonal surface chlorophyll variability, but that seasonal variations of the mixed layer depth-controlled chlorophyll variability due to light limitation. Other physical processes, such as horizontal and vertical advection associated with mesoscale dynamics may also play an important role. Several authors have emphasized the importance of mesoscale dynamics in nutrient and

* Correponding author at: Interdisciplinary Center for Aquaculture Research, Universidad de Concepción, O´Higgins 1695, Concepción, Chile.

http://dx.doi.org/10.1016/j.csr.2017.08.013
Received 17 February 2017; Received in revised form 19 July 2017; Accepted 19 August 2017
Available online 20 August 2017

chlorophyll transport to oligotrophic zones away from the coast. Gruber et al. (2011) showed that high levels of eddy activity tend to be associated with low levels of biological production in the California EBUS, and highlighted that reductions in production and export result from eddy-induced nutrient transport from the nearshore environment to the open ocean. Resplandy et al. (2011) and José et al. (2014) used biophysical modeling to suggest that lateral eddy advection is partly responsible for nutrient provision and distribution. Mesoscale eddies in the HCS appear to contribute significantly with nutrients and chlorophyll to the coastal (< 200 km) and transition zones (up to 80°W) (Correa-Ramírez et al., 2007, 2012; Grob et al., 2003; Morales et al., 2012, 2013), while horizontal Ekman transport and Ekman pumping (i.e. large-scale vertical advection) might act synchronously to extend high concentrations of chlorophyll into the offshore area (Morales et al., 2013). In addition to the physical mechanisms that determine the distribution of nutrients and chlorophyll in the ocean, the availability of different macro and micronutrients and their role in co-limiting phytoplankton growth are also important regulating factors (Messié and Chávez, 2015).

Nutrient availability in the euphotic zone depends on various factors. In the southern Humboldt Current System off central-southern Chile (30–40°S), the injection of nutrients into the mixed layer due to upwelling is partly responsible for high reported primary production rates (Daneri et al., 2000; Montero et al., 2007). Rivers however, such as the Bio-Bio and Itata, also provide important quantities of terrestrial organic matter (Vargas et al., 2012), trace metals and nutrients (anthropic and natural) (Salamanca and Pantoja, 2009) to the inner continental shelf, which enhances the microbial food web as a consequence of the high rates of primary production, mainly provided by the pico- and nanoplankton (Iriarte et al., 2012). Depending on nutrient availability, co-limitation of nutrients occurs when two or more nutrients have been depleted simultaneously down to levels where the addition of one or several is necessary to stimulate phytoplankton growth (Moore et al., 2013).

Nutrient limitation has been reported for some EBUS (Messié and Chávez, 2015). Studies in the Peru upwelling system have shown that iron limits phytoplankton in winter (Bruland et al., 2005; Hutchins et al., 2002); while nitrate and silicate are limiting in summer (Echevin et al., 2008; Messié and Chavez, 2015). In the California EBUS, iron exerts fundamental control over nitrate and silicate drawdown (Hutchins et al., 1998). Iron limitation, for instance, generates blooms of strongly silicified and faster sinking chain-forming diatoms (Hutchins and Bruland, 1998). Iron-stressed diatoms deplete surface waters of silicic acid before they deplete nitrate, leading to the secondary silicic acid limitation of the phytoplankton community (Hutchins and Bruland, 1998).

In some EBUS with large OMZs (Oxygen Minimum Zones), phytoplankton growth has been found to be nitrogen-limited. Kuypers et al. (2005) showed that the anammox process in the Benguela EBUS is the main cause of fixed inorganic nitrogen loss. Quiñones et al. (2010) reported a nitrogen deficit compared to phosphorous in several areas of the HCS, suggesting that primary production may be limited by this element. The authors developed nutrient budgets covering the entire HCS and found $\Delta N/\Delta P$ ratios significantly lower than the expected Redfield values off Chile in three regions: 18–27°S (50 km offshore limit), 27–33°S (50 km offshore limit) and 33–42°S (120 km offshore limit).

An understanding of phytoplankton growth must integrate a number of elements, including physical processes, light and nutrient availability. Untangling the most relevant biogeochemical and physical processes that generate the spatial and temporal variability of plankton remains a major challenge that can be addressed with biophysical modeling.

A number of authors have used biophysical modeling to study biophysical relationships in EBUS focused on nutrients, plankton and primary production, such as: (i) the role of specific physical forcing like tides and storms in the cross-shore transport of nutrients, primary production and chlorophyll in the Canary EBUS (Giraud et al., 2008); (ii) the role of the residence time of nearshore waters and mesoscale activity in different EBUS and their impact on net primary production (Lachkar and Gruber, 2011); (iii) the response of nitrogen, phytoplankton, and zooplankton to circulation driven by summer winds in the HCS (Baird et al., 2007).

The objectives of this study are to (a) assess the realism of a high-resolution coupled physical-biogeochemical regional model for the HCS (30–40°S; 70–80°W) using *in situ* and satellite observations; (b) use this model to characterize the spatial and temporal variability of nutrients potentially limiting phytoplankton growth in this region; and (c) determine the main physical mechanisms (horizontal, vertical advection, vertical mixing) involved in the transport of nutrients to the euphotic layer at the seasonal scale.

2. Methods

2.1. Hydrodynamic model

The hydrodynamic model used in this study is ROMS-AGRIF (Regional Oceanic Modeling System - Adaptive Grid Refinement in FORTRAN, Schepetkin and McWilliams, 2005; Penven et al., 2006; http://www.romsagrif.org).

Simulations were carried out on a grid between 29°S and 41°S, and from 69°W to 83°W (Fig. 1), with a resolution of 7.5 km and 32 sigma levels. The initial and open boundary fields were obtained from a monthly climatology from a Peru-Chile model simulation (Colas et al., 2012) using the "Roms2Roms" offline interpolation package (Mason et al., 2010). The model configuration and atmospheric forcing were described in an earlier study that also evaluated the simulations (Vergara et al., 2016).

2.2. Biogeochemical model

The PISCES (Pelagic Interactive Scheme for Carbon and Ecosystem Studies, Aumont et al., 2003; Aumont and Bopp, 2006; Aumont et al., 2015) biogeochemical model was chosen to represent phytoplankton variability and nutrient co-limitation along the Chilean continental platform. PISCES simulates the cycles of carbon, oxygen and the main nutrients that control phytoplankton development (PO_4^{3-}, NO_3^-, NH_4^+, Si, Fe). In this model phytoplankton growth depends on external nutrient concentrations. It includes two phytoplankton classes (diatoms and nanophytoplankton) and two zooplankton classes (micro and mesozooplankton). There are three non-living compartments: semi-labile dissolved organic matter, small sinking particles and large sinking particles. A detailed description of the model structure and equations can be found in Aumont et al. (2015).

PISCES coupled to ROMS has been used for the Peru upwelling system to address questions over different time scales, such as the impact of climate change on the survival of small pelagic fish larvae (Brochier et al., 2013), the impact of intraseasonal coastal-trapped waves on the nearshore Peru ecosystem subsurface (Echevin et al., 2014), and the processes that control the seasonal cycle of chlorophyll in the northern Humboldt Current System (Echevin et al., 2008).

The biogeochemical fields of the model (nitrate, phosphate, silicate, oxygen, DIC, DOC, alkalinity) were initialized in the domain and imposed at the model's open boundaries using CARS 2009 climatology (CSIRO Atlas of Regional Seas, http://www.marine.csiro.au/~ dunn/cars2009/, Ridgway et al., 2002). Due to the scarcity of data, Fe concentrations were obtained from a global climatology model (ORCA2-PISCES, Aumont et al., 2015). Iron data was also obtained from a three-dimensional atmospheric dust deposition model (Tegen and Fung, 1995) and from a time-constant depth-dependent sediment mobilization model (Moore et al., 2004).

Limitations due to light and nutrients were quantified by calculating

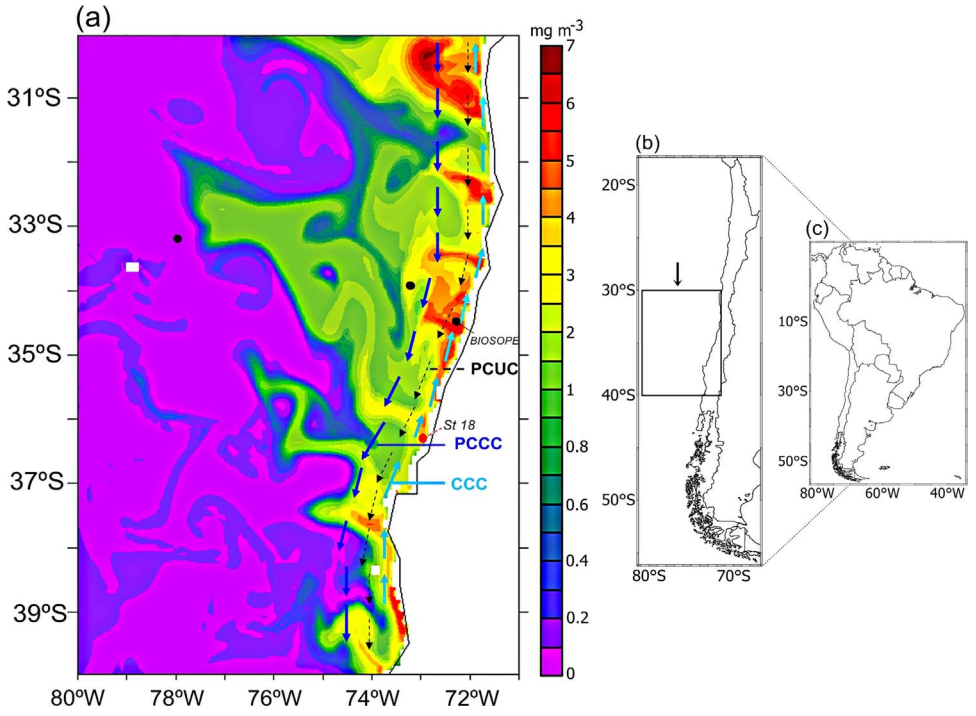

Fig. 1. (a) ROMS-PISCES model domain. Modeled surface chlorophyll (in mgChl m^{-3}, color scale) is shown (January of Year 10). The main surface (CCC, light blue arrow, and PCCC, dark blue arrow) and subsurface (PCUC, black dashed arrow) nearshore currents of the HCS are indicated. Station 18 is marked by a red dot, and the BIOSOPE stations for Fe measurements are denoted by black dots. (b) and (c) correspond to maps of Chile and South America, respectively. Rectangle in (b) indicates the location of the study area.

the limiting terms in the model parameterization of primary production (Aumont et al., 2015). Primary production in the model is proportional to the limiting terms of light and nutrients. The light limitation term (L_{light}) is (1-exp (-α (Chl/C))) * PAR/(μL_{nut})), where α is the initial slope of the PI curve, Chl/C is the chlorophyll/carbon ratio, PAR is photosynthetically active radiation, and μ is the temperature-dependent development rate. PAR is computed using COADS (da Silva et al., 1994) climatological shortwave flux. When sufficient light is available this term reaches 1, and is less than 1 when light limits development. Nutrient limitation L_{nu} is equal to min $_{i\ =\ 1...n}$ [C_i/(K_i + C_i)], where i is the index indicating a specific nutrient (PO_4^{3-}, NO_3^-, NH_4^+, Si, Fe), C_i is the concentration of the nutrient, and K_i is its saturation constant. The limiting terms were calculated for diatoms, since this group is the main contributor to total chlorophyll in the study zone. The so-called "limiting nutrient" in our study is the one (i_0) with the lowest ratio (C_i/(K_i + C_i) ≤ C_i/(K_i + C_i)).

Runoff from Chilean rivers (e.g. the Biobio and Itata Rivers, both near 36°S) was not explicitly incorporated in the simulation. The impact of river discharge on salinity was represented owing to relaxation of climatological sea surface salinity (see Vergara et al., 2016). However, riverine nutrient input was not taken into account.

To determine the physical mechanisms that transport nutrients in the euphotic layer, advection (zonal (-U∂_xC), meridional (-V∂_yC) and vertical (-W∂_zC)), and vertical mixing (∂_z(K∂_zC)) were computed, where U, V, W are zonal, meridional and vertical velocity terms respectively, K is the vertical diffusivity, C the nutrient concentration, and x, y, z the zonal, meridional, and vertical (oriented upward) coordinates, respectively. The transport terms were stored online and averaged every 3 days. Only the silicate transport terms were analyzed as silicate was the main limiting nutrient (see Section 3.4).

We ran ROMS/PISCES simulations for 15 years, including a 5-year spin-up period. The last 10 years of the simulations were averaged to obtain the seasonal climatology of the biological variables. The biological parameters used were similar to those listed in Echevin et al. (2014).

2.3. Data used to evaluate the model

One of the parameters estimated by ROMS is the height of the boundary layer (HBL), also named mixed layer depth (MLD). The MLD is considered as the region near its surface with vertically quasi-uniform oceanic tracers above a layer of more rapid vertical changes (Lorbacher et al., 2006). In the MLD there is little variation in salinity, temperature or density with depth (Kara et al., 2003; Pickard and Emery, 1990). The MLD is created by turbulence generated by the wind, convective cooling, breaking waves, current shear, and other physical processes and characterized by vertically uniform and intense mixing (Wijesekera and Gregg, 1996).

The parameterization of the boundary layer mixing in ROMS follows the formulation of Large et al. (1994). The boundary layer height was determined based on the dimensionless Richardson number Ri (i.e. the ratio between buoyancy and the vertical shear of horizontal velocity). The modeled mixed layer depth was compared to climatological MLD from de Boyer Montégut et al. (2004), which has a regular grid of 2 × 2° with a monthly resolution. The climatological MLD was based on individual profile estimates. The criterion selected is a threshold value of temperature or density from a near-surface value at 10 m depth (ΔT = 0.2 °C or Δσθ = 0.03 kg m^{-3}).

Surface chlorophyll concentrations were provided by SeaWiFS satellite data (http://oceancolor.gsfc.nasa.gov/SeaWiFS/) over the 2000–2006 period. The satellite data was compared with the model simulation.

A monthly climatology of in situ nitrate, phosphate, silicate, and chlorophyll data from Station 18, located in the central-southern Chilean shelf (36.5°S; 73.1°W; see Fig. 3a), over the 2004–2014 period was compared with the simulation. Station 18 is a time series initiated by the COPAS Oceanographic Center in 2002, located on the shelf at 88 m depth (Escribano and Schneider, 2007).

3. Results

3.1. Evaluation of mixed layer depth

The annual mean mixed layer depth (MLD) of the model was compared to the climatology in Fig. 2. The MLD was shallower nearshore than offshore due to enhanced stratification near the coast associated with nearshore upwelling of dense water (Sobarzo et al., 2007). The observed MLD was between 28 and 34 m nearshore and deeper

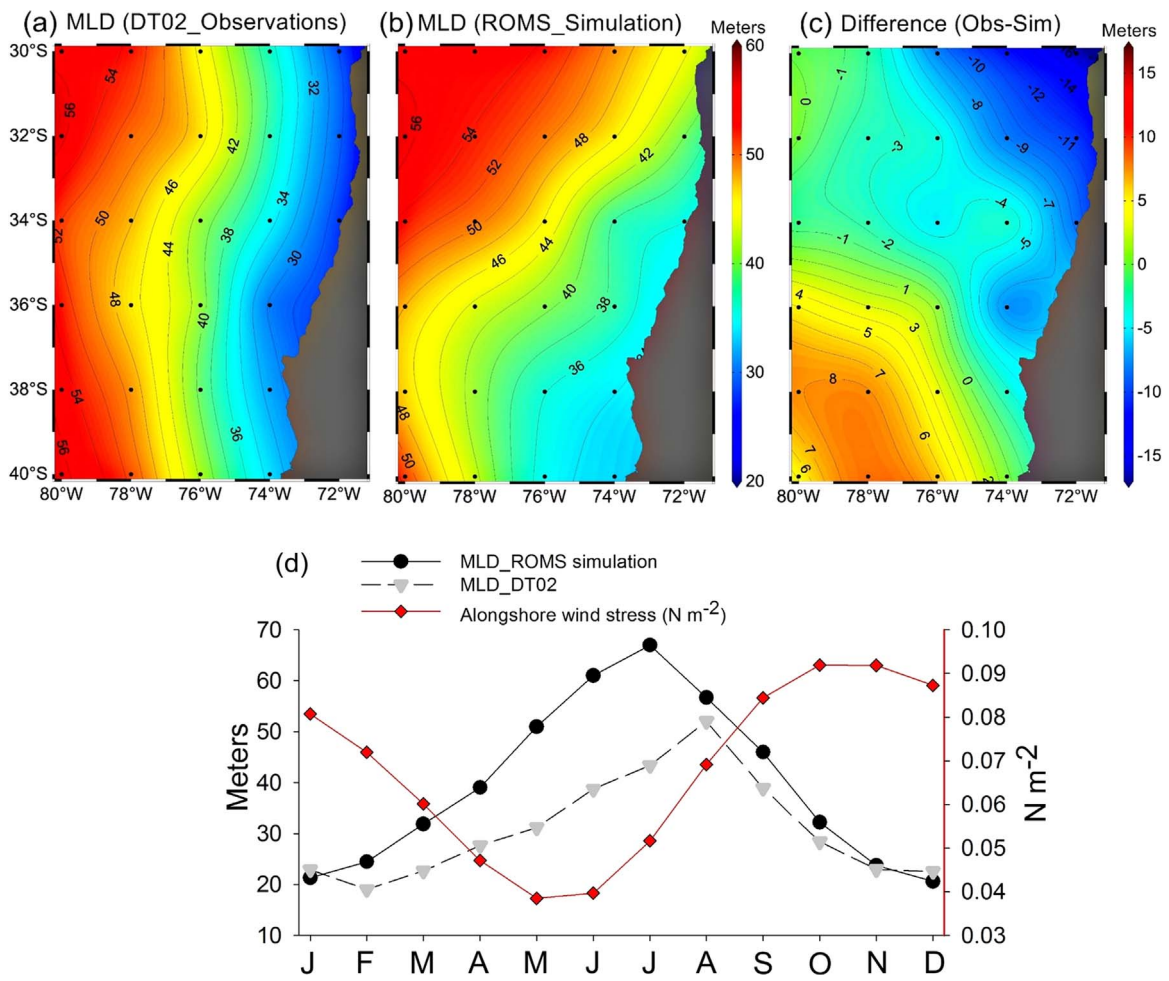

Fig. 2. Annual mean mixed layer depth (MLD, in meters) estimated by (a) de Boyer Montégut et al. (2004) climatology (2° × 2°), (b) ROMS model climatology (averaged on a 2° × 2°) and (c) differences between observations and simulation. Black dots represent the 2°x2° regular grid. (d) Annual cycle of modeled (black circles) and climatological (grey triangles) MLD (in meters) and alongshore wind stress (in N m^{-2}, red diamonds) within a band of 100 km between 30° – 38°S.

than 50 m offshore (Fig. 2a). Near the coast, the modeled MLD ranged from 34 to 38 m and deepened offshore (> 50 m) (Fig. 2b). The greatest differences between the model and observations were found in the north of the study area (Fig. 2c). The largest discrepancies near the northern boundary could be an effect of open boundary conditions.

The modeled and observed annual MLD cycle (averaged in a 100-km band from the coast) are shown in Fig. 2d. The modeled MLD for spring and summer was about 20 m, and was deeper (~ 50–60 m) for autumn and winter. The observed MLD had similar values in summer and higher values in winter, fluctuating between 40–50 m. Although the annual cycles of the modeled MLD and the observed MLD series were similar, the model values of the MLD were deeper than those observed, mainly in autumn and winter (from May to August).

3.2. Distribution and annual cycle of surface chlorophyll

Both maps of modeled and observed surface chlorophyll showed high values near the coast in a band of approximately 100 km, decreasing gradually offshore (Fig. 3a and b). However, observed values reached concentrations close to 10 mg Chl-a m^{-3} (Fig. 3b), whereas modeled values did not exceed 3 mg Chl-a m^{-3} (Fig. 3a). The zones with the highest chlorophyll concentrations were between 34° and 37°S, and between 38° and 40°S (Fig. 3a and b).

The time-latitude plots of surface chlorophyll (averaged in a 100-km coastal band) showed that the highest concentrations were in spring and summer (Fig. 3c and d), as S-W winds favorable to upwelling predominated (Fig. 2c). The maximum values of modeled chlorophyll were 3.5 mg Chl-a m^{-3} (Fig. 3c), while observed values reached 6.5 mg Chl-a m^{-3} (Fig. 3d). The highest modeled and observed concentrations were found between ~ 33° and 37°S (Fig. 3c and d). In both the model and SeaWIFS data, a sharp change in chlorophyll concentration was found near Punta Lavapie (37.2°S), the southern limit of the Gulf of Arauco, and chlorophyll values decreased south of this latitude.

Chlorophyll values from SeaWIFS and from the simulations were compared at Station 18 (Station 18, 36.5°S; 73.1°W; see Fig. 1). The three datasets showed roughly similar annual cycles, with the highest concentrations in spring and summer months (Fig. 4a). Modeled chlorophyll concentrations for summer were underestimated. Chlorophyll decreased in autumn and winter in the three datasets, reaching ~ 2 mg Chl-a m^{-3}. There was, however, a time difference between the modeled minimum concentration in July-August and the observed minimum was in June-July.

We also evaluated the annual cycle of the vertical structure of chlorophyll at Station 18. The two data sets had relatively similar vertical structures, with a chlorophyll-rich (> 1 mg Chl-a m^{-3}) layer of ~ 20–30 m depth. However, modeled chlorophyll did not exceed 4 mg Chl-a m^{-3} (Fig. 4b), while it reached ~ 11 mg Chl-a m^{-3} at Station 18 (Fig. 4c). Another important difference is the progressive thickening of the modeled chlorophyll-rich layer from 20 m (March) to ~ 50 m (July), whereas observations exhibited an abrupt decrease in chlorophyll content, with values of ~ 0.2 mg m^{-3} in July and a progressive thinning of the surface chlorophyll-rich layer from ~ 30 m (January) to

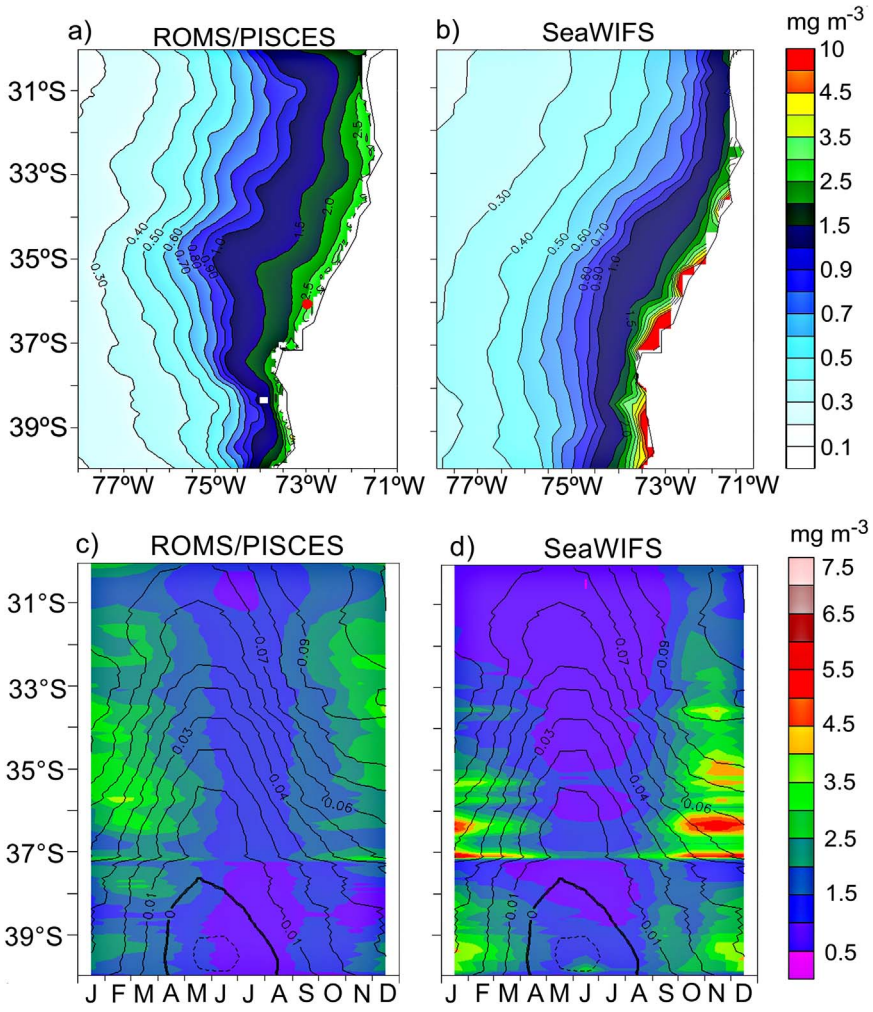

Fig. 3. Annual mean surface chlorophyll (in mg Chl-a m^{-3}) estimated by (a) the model (red circle: Station 18) and (b) SeaWIFS observations (1998–2006). Annual cycle of surface chlorophyll within a 100 km coastal band in (d) the model, and (e) SeaWIFS. Annual along-shore wind stress (in N m^{-2}) cycle is superimposed.

~ 20 m (April).

3.3. Nutrients

The simulated phosphate, nitrate and silicate were compared to observations at Station 18 (Fig. 5). The annual cycles of the three nutrients were similar, with the highest values in spring and summer at the surface layer depth (~ 20 m), probably associated with upwelling. Discrepancies between the model and observations were found. The maximum concentration of PO_4 (~ 2.8 μM) at Station 18 (Fig. 5b) was greater than that of the model, the latter not exceeding 2.2 μM (Fig. 5a). The highest modeled nitrate values (~ 32.5 μM) were at 80 m depth (Fig. 5c), while maximum observed NO_3 was only ~ 27 μM (Fig. 5d). The high nitrate values could be due to a lack of denitrification caused by excessively high oxygen values in the model (figures not shown). Silicate concentration values for the model and Station 18 observations were similar, fluctuating between ~ 5 and 30 μM (Fig. 5e and f). The highest concentrations were found between 40 and 80 m depth. However, there was a slight increase in the silicate surface concentration at Station 18 (0–10 m) in July and August (Fig. 5f), which was not simulated by the model. This is likely due to local river nutrient discharges that were not taken into account in the model.

Although data on Fe for the study region are scarce, we used three vertical profiles of Fe measured during the BIOSOPE cruise (Blain et al., 2008; Bonnet et al., 2008) to evaluate modeled Fe concentrations (Fig. 6). The profiles were located on a cross-shore section (between 33.4° and 34.5°S) off central Chile. The offshore measurements (78.1°W) had low surface values (< 0.05 nM between 50 m and 100 m depth), in agreement with the model. Modeled subsurface values were fairly close (bias is less than 0.05 nM) to the observed values. The "nearshore" measurements (73.5°W) showed higher concentrations than offshore, with values near 0.05 nM in the surface layer and greater than 1 nM at depths between 150 m and 400 m. In contrast, the surface values of the modeled profile were slightly greater (~ 0.07 nM) than those observed and increased moderately, reaching 1 nM at 400 m depth. The "coastal" profiles displayed the strongest discrepancies. Modeled Fe in the surface layer (0–30 m) reached 2.2 nM and decreased to 1.5 nM at ~ 80 m depth, while observed Fe between 30 m and 80 m was around 1.2–1.3 nM. Modeled Fe remained relatively unchanged (~ 1.2–1.3 nM) below 100 m depth, in contrast with observed Fe, which was over 3 nM at depths between 150 m and 300 m. While year-to-year variability of modeled Fe was strong (σ ~ 1 nM, figures not shown) between 0 and 100 m, modeled Fe at greater depths was never higher than 1.5 nM.

3.4. Co-limitation of nutrients and light for diatoms

3.4.1. Surface co-limitation

Since diatoms are the main contributor to total chlorophyll (70%) (Figure not shown), the co-limitation of nutrients was only computed for this phytoplankton group. As the differences among different simulation years of the co-limitation of nutrients and light were not significant, we chose the 12 months of a typical simulated year (Year 10) and computed co-limitation fields from 0 to 20 m depth to study seasonal variations. To highlight the presence of eddies, we superimposed the Sea Level Anomaly (SLA).

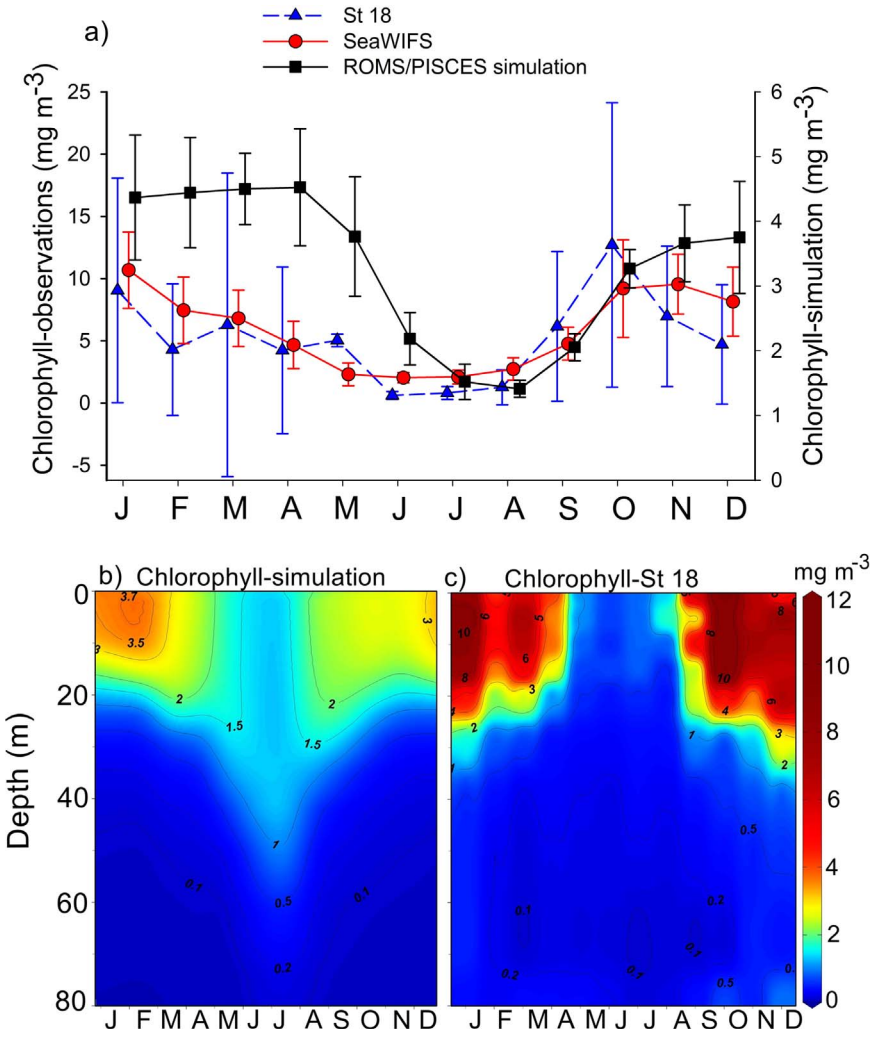

Fig. 4. Seasonal cycle of surface chlorophyll for (a) Station 18 (36.3°S; 73°W; see location in Fig. 1) *in situ* data (blue triangles), SeaWIFS satellite data (red circles) and the simulation (black squares). Seasonal cycle of chlorophyll between 0 and 80 m for (b) the model and (c) Station 18 *in situ* data.

Co-limitation patterns displayed complex structures (Fig. 7). The main limiting nutrients were silicate, Fe and nitrate, with occasional small-scale patches of P limitation. Silicate and Fe were limiting mainly near the coast (~ 100 km) from January to April (Fig. 7a–d), with predominantly silicate limitation. During these same months, nitrate was limiting further from the coast, from ~ 75°W to 80°W. Light was limiting near the coast, as nutrients were more abundant nearshore due to upwelling. Light limitation occurred over a narrow band (< 100 km) in summer, which increased in winter due to decreased insolation (Hernández et al., 2012). The spatial extension of light and silicate limitation increased throughout the coastal zone from May to August (Fig. 7e–h), overlapping with nitrate limitation (May and June). Fe limitation increased from September to December, especially in November, extending away from the coast. Phosphate limitation decreased notably during these months (Fig. 7i–l).

Eddies were observed during all analyzed months, and may have transported the most important nutrients (i.e. nitrate, phosphate and silicate) from the coast to the ocean (Fig. 7). Co-limitation patterns and seasonal evolution in mesoscale eddies were apparent. Several cyclones with a predominant Fe limitation in their core occurred in summer and fall (Fig. 7a–d). In late fall and winter, nutrient limitation in the eddy cores shifted from Fe to Si (Fig. 7e–h), with the presence of ribbons of Fe and P limitation around the core (Fig. 7i), revealing a high degree of complexity.

3.5. Silicate transport

3.5.1. Advection, mixing and silicate trends from 0 to 20 m depth

Silicon was the most important limiting nutrient for diatoms in the coastal zone (Fig. 7), which is why we analyzed the balance of this element in terms of advection and vertical mixing. We computed the silicate transport terms in the first 20 m of the water column, as the modeled maximum chlorophyll concentration was observed in the surface layer (Fig. 3b).

Mean Si concentrations fluctuated between 2 and 20 μM, with the highest values (> 10 μM) in the coastal zone between 30° and 37°S due to coastal upwelling (Fig. 8g). Si values were higher in the north of the region as the PCUC transported upwelled source waters poleward. As expected, annual mean vertical advection of Si was mainly positive near the coast due to coastal upwelling (Fig. 8a). Highest values ($> 5.10^{-5}$ μM Si s^{-1}) were found in few areas of the northern part of the study area, from about 30° to 35°S (Fig. 8a). The horizontal advection terms displayed more complex small-scale patterns. Zonal advection was mostly negative offshore in a ~ 100 km coastal band and was positive near the coast (Fig. 8b). Meridional advection was mostly positive offshore (Fig. 8b) and negative in a narrow (< 20 km) coastal strip, which was consistent with the equatorward coastal flow (Fig. 8d) and the presence of less rich waters in the south (Fig. 8g). The signature of permanent mesoscale eddies and jets was observed between 30° and 35°S (Fig. 8d). This means that while vertical advection brought nutrients to the coastal area, Ekman currents and enhanced offshoreward jets near 32°S, 33°S, 34°S (Fig. 8d) transported part of the high coastal

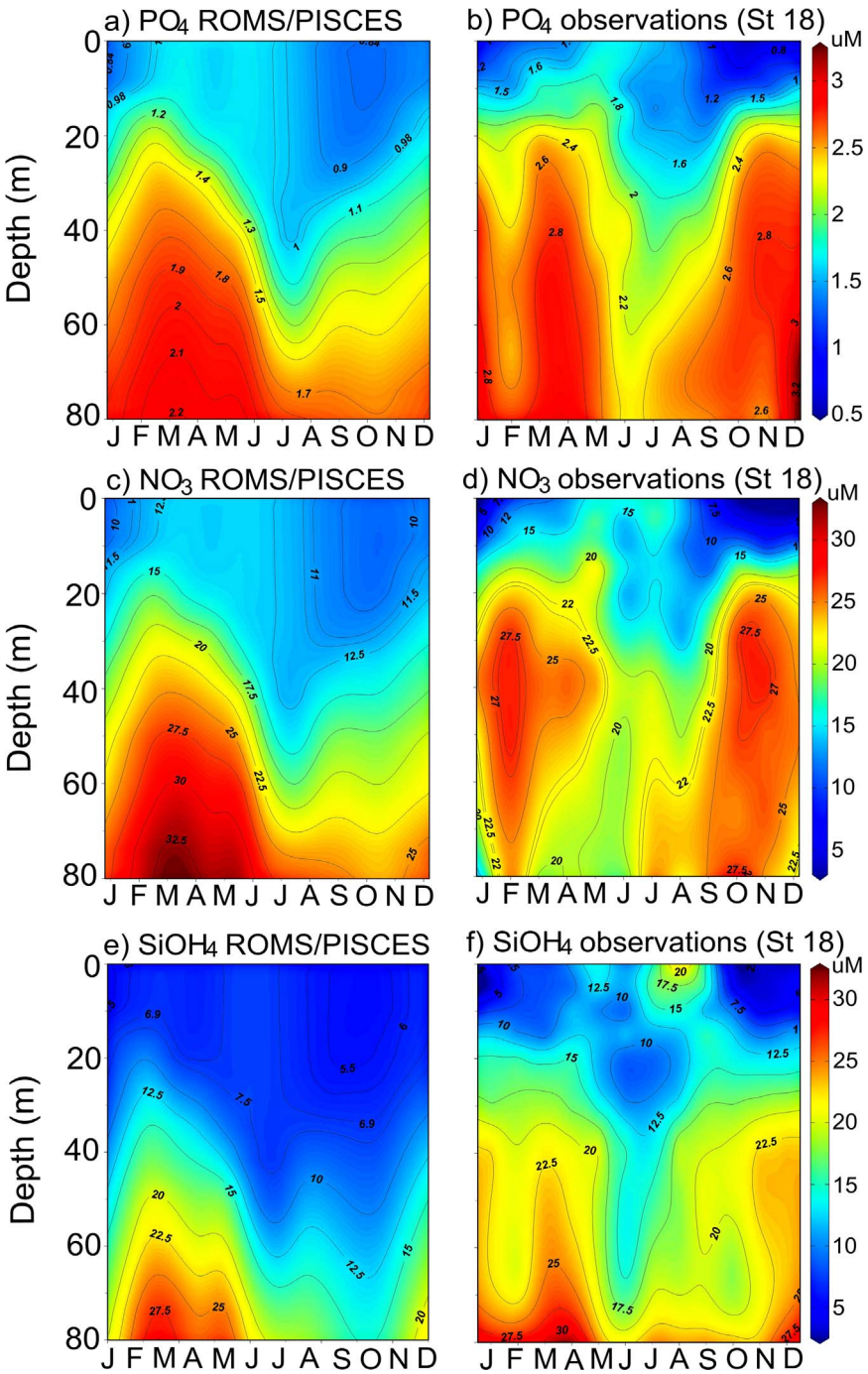

Fig. 5. Seasonal cycle of (a) Modeled phosphate, (c) nitrate and (e) silicate versus observed values (b, d, f) at Station 18. Units are $\mu mol\, l^{-1}$.

nutrient load offshore (Fig. 8g), thus partly compensating for the vertical input associated with coastal upwelling (Fig. 8e). Total positive advection predominated in the study area, with highest values (~ 3–5 10^{-6} μM Si s-1) at ~ 32°, 36° and 37°S (Fig. 8e). The input of nutrients through vertical mixing was positive everywhere, and greater than through advective fluxes in the offshore regions (50 km from coast) between 30°S and 35°S (Fig. 8f).

Fig. 9 shows the sum of the physical trend, biological trend and total trend of silicate in the study zone. As expected, the physical trend was positive throughout the study zone, with highest values between 30° and 37°S (Fig. 9a). The negative biological trend (primary production is a Si sink) displayed similar patterns to those of the physical trend (Fig. 9b). The total trend was mostly positive, but values were an order of magnitude smaller than those of the physical and biological trends (Fig. 9c), indicating that the model had not reached a fully equilibrated statistical state after 15 years. Nevertheless, moderate Si drift (see also Fig. 10) suggests that a longer simulation would not significantly alter the result.

3.5.2. Cross-shore structure of currents and Si transport terms

Figs. 8 and 9 show that the zone between 31° – 37°S had the highest values of advection and physical and biological trends of silicate. To study the vertical structure of Si transport in the water column, we averaged the velocity components and transport terms meridionally between 31° and 37°S (Fig. 10). Similar diagnostics were performed in Colas et al. (2012). Cross-sections are displayed between 0 and 100 m depth and 0–200 km from the coast (Fig. 10).

To highlight the relationship between Si transport and velocity

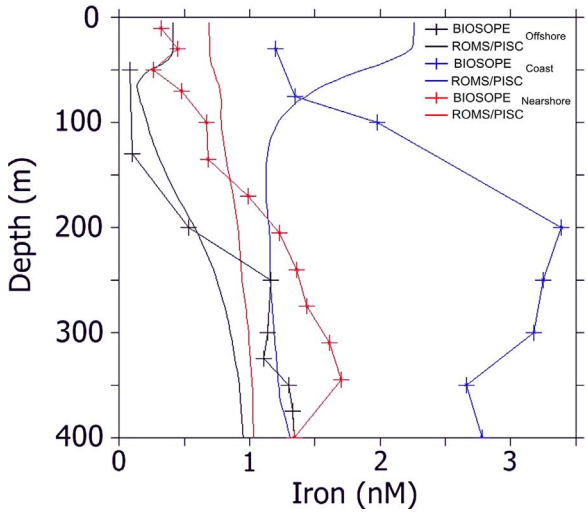

Fig. 6. Iron profiles from model simulations (lines) and BIOSOPE (lines with crosses) measurements (Blain et al., 2008; Bonnet et al., 2008) at three stations (see location in Fig. 1): "offshore" (33.36°S, 78°W; black), "nearshore" (33.8°, 73.5°W; red) and "coastal" (34.5°S; 72.4°W; blue) profiles.

patterns, vertical sections of annual mean zonal (u, Fig. 10b), meridional (v, Fig. 10d) and vertical velocity (w, Fig. 10g) are shown. The wind-driven offshoreward Ekman current associated with the coastal upwelling was reflected in negative zonal velocity (u) in the surface layer (0–15 m). The subsurface zonal velocity was positive in two areas, one close to the coast (from 10 to 50 m depth) with values > 0.5 ms^{-1}, and the other one at 100–200 km from the coast (from ~ 15–100 m depth). The positive velocity likely corresponded to the shoreward current compensating upwelling. The negative subsurface core located 60 km from the coast could have been produced by the poleward undercurrent, which was deflected slightly westward by the coastline orientation.

Meridional velocity (v) (Fig. 10d) near the coast was positive and associated with the Chile Coastal Current (CCC; Mesias et al., 2001; Strub et al., 1998; Fig. 1), which flows towards the equator. Below this current, poleward flow is associated with the PCUC (Peru-Chile Undercurrent; Huyer et al.,1991; Silva and Neshyba, 1979; Fig. 1), which was trapped on the continental platform between 40 and 100 m. The PCUC extended to 100 km offshore. The poleward flow from ~ 120–200 km was associated with the PCCC (Peru-Chile Countercurrent, Strub et al., 1995). As expected, vertical velocity (w) (Fig. 10g) was positive throughout almost the entire study section, with the highest values near the coast (> 0.5 ms^{-1}).

Zonal advection was predominantly negative in the surface layer (0–100 m) (Fig. 10e). The negative subsurface pattern was associated with the PCUC, which was southwestward due to the coastline orientation between 31° and 37°S, and thus projected zonally as a westward current transporting nutrients offshore. The surface pattern (0–10 m) of zonal advection is more complex to interpret. It was negative nearshore (< 100 km) and positive offshore (100–200 km). Note that the annual nearshore average of U was negative (Fig. 10d) and the annual mean cross-shore Si gradient (∂_xSi) was positive as Si concentrations increased towards the coast (Fig. 10a). Consequently, transport associated with the mean current and mean Si gradient (-U.∂_xSi) was positive (figure not shown), while total (*i.e.* eddy + mean) zonal advection was negative (Fig. 10e), suggesting that eddy fluxes play an active role by depleting the nearshore layer and enriching the offshore region (*e.g.* Gruber et al., 2011).

Meridional advection (Fig. 10c) was mainly positive, except for two zones with negative values close to the coast (~ 10 km), and between 90 and 120 km. Positive values can be associated with the undercurrent (Fig. 10b), which transports nutrient-replete waters poleward along the coast. In contrast, the equatorward coastal surface jet (Fig. 10b) transported relatively nutrient-poor Si surface waters northward (Fig. 8g), acting as a silicate sink (Fig. 10c).

Horizontal (*i.e.* zonal + meridional) advection (Fig. 10f) was negative near the coast, with values lower than -6 μM Si month^{-1}. Two positive zones were found, between about 100 and 200 km offshore, and near the coast at less than 60 m (Fig. 10c). Vertical advection (Fig. 10h) was mainly positive (> 6 μM Si month^{-1}) from the coast to 140 km offshore. Vertical mixing was a source of Si in the first 20 m depth from the coast to 200 km, with values greater than 6 μM Si month^{-1} and a sink below 20 m depth (Fig. 10i). Vertical mixing was confined to the 0–50 m depth layer. It served to mix nutrient-rich subsurface waters with less rich surface waters (0 −10 m), enriching the surface waters. Total advection (Fig. 10j) was positive from the coast to 200 km offshore in the first 50 m of the water column, with transport values > 2 μM Si month^{-1}, and slightly negative at greater depths. The sum of all physical terms (*i.e.* advection + vertical mixing; Fig. 10k) was positive between 0 and ~ 30 m depth, with values > 2 μM Si month^{-1}, and slightly negative below 30 m. The total trend (physical + biological trend) (Fig. 10l) was mainly positive and weak (< 0.2 μM Si month^{-1}) in comparison with other terms, with slightly higher values near the coast.

3.5.3. Annual cycle of silicate balance

The annual cycles of the transport and biological terms were averaged over a coastal band of 100 km (Fig. 11a) and over an offshore band of 100 km (Fig. 11b), between 0 and 20 m depth, to study their relationships with the annual chlorophyll cycle. We considered the latitudinal zone from 31° to 37°S. Vertical mixing and vertical advection in the coastal band (Fig. 11a) were positive throughout the year and showed similar annual cycles, with higher values in spring and summer, and lower in autumn and winter, as expected from the seasonal cycle of surface winds (Fig. 2c). Horizontal advection was mainly negative, with values close to zero in autumn-winter and lower values in spring-summer (Fig. 11a). The annual cycle of total advection was similar to that of horizontal advection, but with a weaker amplitude, higher values in autumn-winter and lower values in spring-summer, and a predominance of positive values (Fig. 11a). Interestingly, vertical nutrient advection reached maximum positive values during the peak of the upwelling season (January-February), but was nevertheless offset by very strong offshore advection, possibly enhanced by eddy effects (Fig. 12) and resulting in negative values.

The total physical trend was always positive within the coastal band, with greater values in autumn-winter. The biological trend was always negative, with lower values in spring-summer (~ 1.5 10^{-6} μM Si s^{-1}) compared with autumn-winter (~ 2.5 10^{-6} μM Si s^{-1}). The total trend was weak and constant throughout the year, varying slightly with predominantly positive values (< 0.3 10^{-6} μM Si s^{-1}).

The annual cycle of silicate balance in the oceanic offshore band (Fig. 11b) showed lower values (< 2 10^{-6} μM Si s^{-1}) than near the coast, with different contributions from several processes. In contrast to coastal upwelling, vertical advection was negative year-round. Downwelling was likely due to anticyclonic wind stress curl (Bakun and Nelson, 1991; Aguirre et al., 2012). The highest vertical mixing values were in spring-summer and the lowest in autumn-winter, which was in agreement with the seasonal cycle of offshore wind stress intensity (Figure not shown). Negative vertical advection was partly offset by horizontal fluxes, with higher values from April to September, possibly due to enhanced eddy flux of coastally upwelled nutrients in winter (Fig. 12). In conclusion, nutrient input in the offshore band was mainly achieved through wind-driven vertical mixing in summer and horizontal advection in winter, possibly due to mesoscale eddy propagation (Correa-Ramirez et al., 2007).

In both bands, surface chlorophyll had high values in spring-summer, with greater values (> 2 mg Chl-a m^{-3}) in the coastal band than in the oceanic band (~ 1.6 mg Chl-a m^{-3}, Fig. 11). As

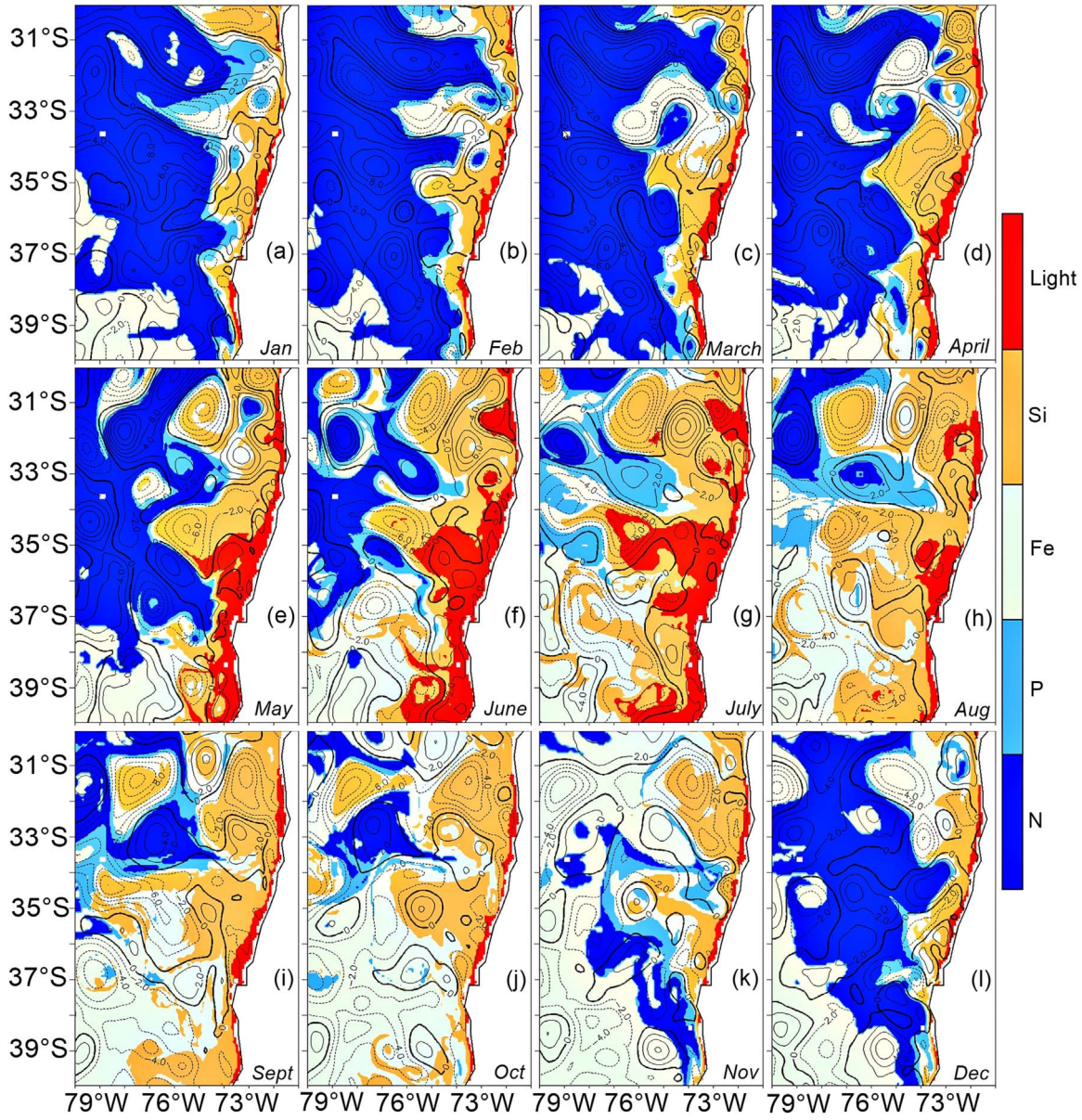

Fig. 7. Maps of surface co-limitation fields during Year 10, from January to December between 0–20 m. Colors indicate whether nutrients or light are limiting. Contours (in cm) represent the sea level anomaly.

phytoplankton growth was mainly limited by light in the coastal band (Fig. 7), surface chlorophyll was largely influenced by vertical mixing and solar radiation seasonality. Therefore, coastal chlorophyll correlated better with the vertical mixing term ($c = 0.77$, $p = 0.005$) and with (-1)*MLD ($c = 0.83$, p-value $= 0.001$) than with the total input of nutrients in the surface layer ($c = 0.54$, $p = 0.075$).

4. Discussion

The aim of this study was to characterize the seasonal dynamics of surface chlorophyll and its relationship to nutrient fluxes in the surface layer. Very few studies in the southern HCS have used biogeochemical-physical coupled modeling to study the relationship between hydrodynamic and biological processes. Baird et al. (2007) used a physical model (POM) (Blumberg and Mellor, 1987) coupled to an NPZ model to investigate the response of the ecosystem to the circulation driven by summer winds in central-southern Chile. These authors studied the impact of biological parameters, such as zooplankton grazing pressure, on the magnitude and spatial distribution of surface chlorophyll. The nearshore spatial resolution (~ 15 km) in Baird et al. (2007) was lower than in our simulations, thus mesoscale eddy effects might have been underestimated in their study. Moreover, they did not simulate a full seasonal cycle, and their biogeochemical model was simpler than the PISCES model. Overall, these differences make it difficult to compare their results with ours.

Our results make a significant contribution to understanding physical-biological coupling in the southern HCS. We found that the modeled surface mixed layer depth (MLD) reproduced observed seasonal variability relatively well (Fig. 2d), becoming deeper in autumn and winter, and shallower in spring and summer. The MLD appeared to be modulated mainly by alongshore wind stress in our study, but other processes not accounted for in our model, such as riverine fresh water fluxes, may also play a role during certain periods of the year (Sobarzo et al., 2007). The nearshore modeled MLD was too deep, which could impact the simulated primary production by a too strong light limitation and decrease surface chlorophyll. Using a ½ ROMS simulation of the Pacific Ocean, Lemarié et al. (2011) computed the MLD using individual temperature profiles and the same criteria as de Boyer

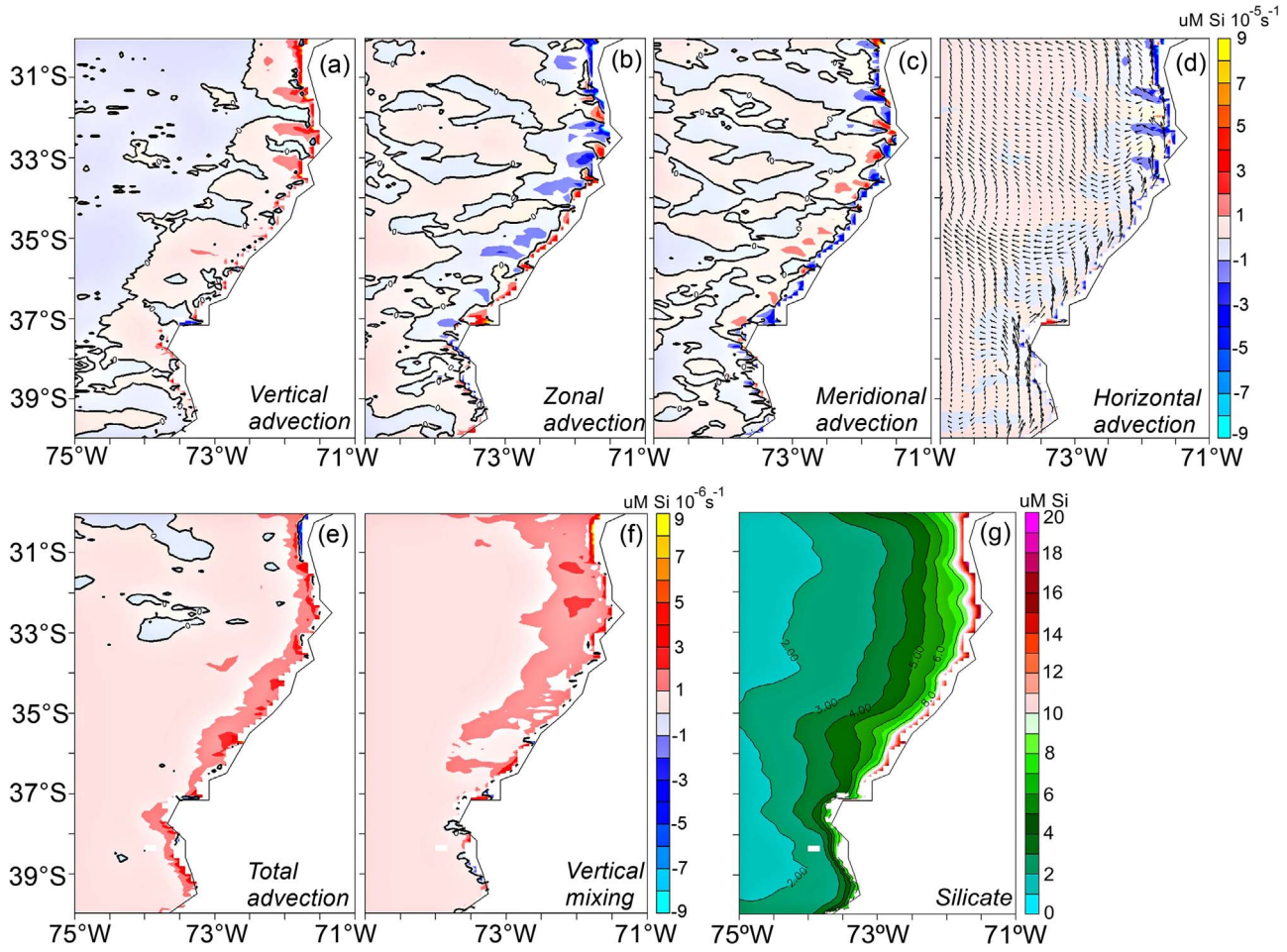

Fig. 8. Annual mean transport terms (in μmol s^{-1}) for silicate advection: vertical (a), zonal (b), meridional (c), horizontal (d), total (e), vertical mixing (f). Annual mean modeled silicate (μmol l^{-1}). All fields are averaged between 0 and 20 m.

Montégut et al. (2004). They also obtained a positive bias (i.e. a too deep simulated MLD off the coasts of Chile, see their Fig. 5). Therefore, the differences between observed and modeled MLD could not be attributed to the different methods used. Using a high frequency (daily or 6-hourly) wind forcing may also impact the MLD, but estimating this effect is beyond the scope of the present model study.

An abrupt change in nearshore chlorophyll concentration at ~ 37°S (Gulf of Arauco) was simulated by the model and also seen in observations (Fig. 3c and d). This high chlorophyll concentration is probably an effect of the local topography. The Gulf of Arauco, an equatorward-facing gulf, favors strong upwelling events because of its geographic orientation, and thus has a high level of biological productivity (Figueroa and Moffat, 2000). This zone of complex bathymetry is also strongly influenced by the submarine canyon of the Bio-Bio River, which modifies coastal circulation and induces upwelling of water from depths greater than 200 m (Sobarzo et al., 2001, 2016). In

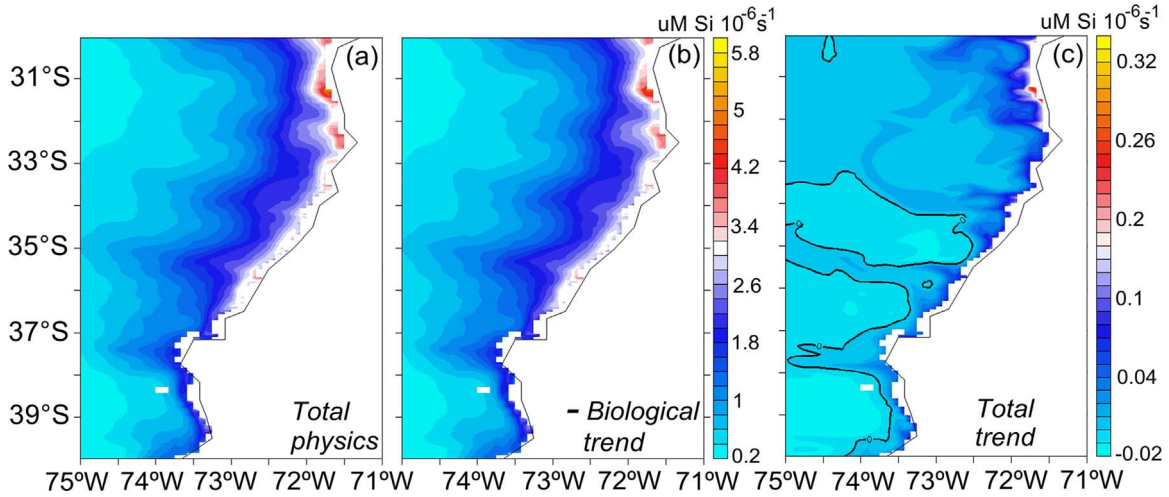

Fig. 9. Total physical trend (a), (−1)x biological trend (b) and total trend (physics + biology) for silicate (in μmol s^{-1}), between 0 and 20 m.

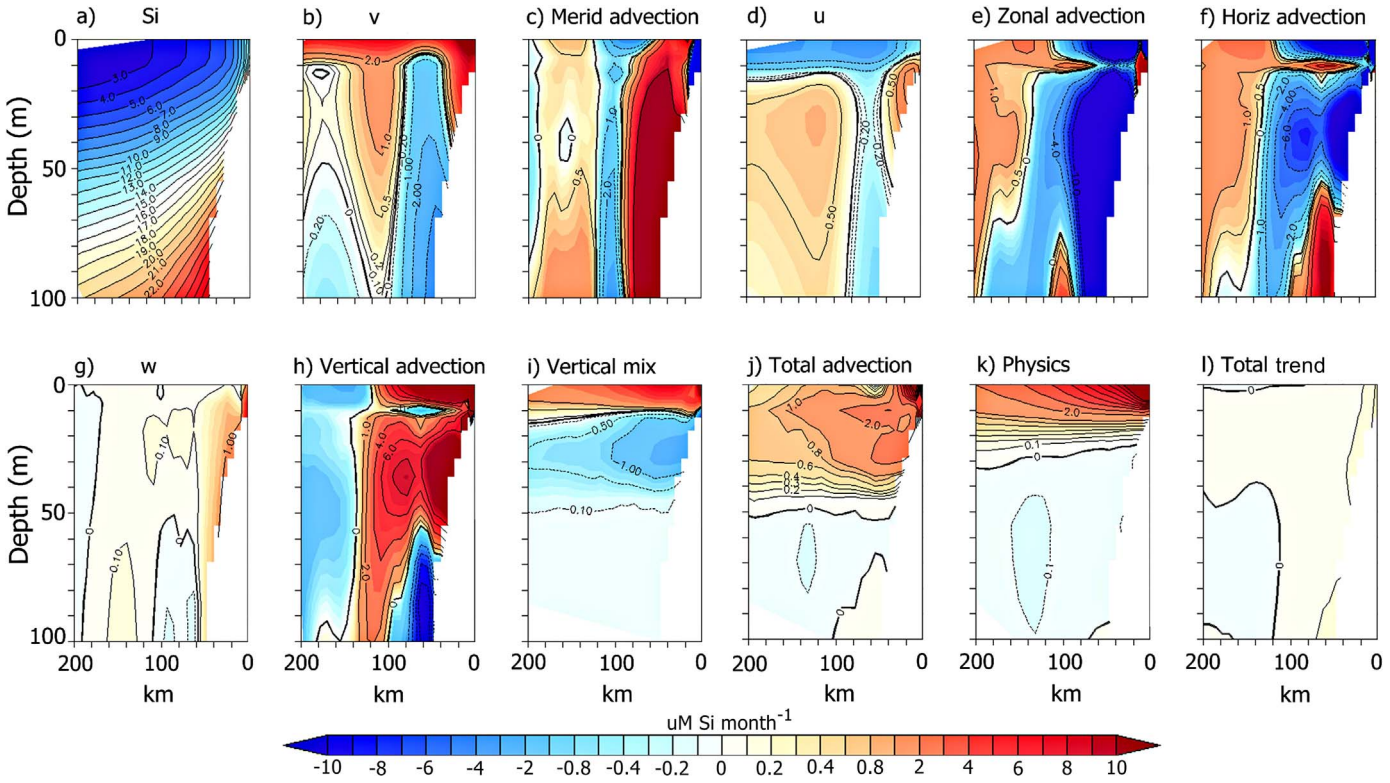

Fig. 10. Along-shore averaged (31° − 37°S) sections of (a) silicate (μmol l^{-1}) and silicate transport terms (in μmol $month^{-1}$): (c) meridional advection, (e) zonal advection, (f) horizontal advection, (h) vertical advection, (i) vertical mix, (j) total advection, (k) total physical trend, and (l) total trend (physics + biology) (j) of silicate between 0 and 100 m from 31–37°S. Alongshore average of (b) zonal (u, in m s^{-1}), (d) meridional (v, in m s^{-1}) and (g) vertical (w, in m s^{-1}) velocity components.

addition, off Lavapie Point (south limit of the Gulf of Arauco), there are strong equatorward currents in the form of an upwelling jet (Atkinson et al., 2002) that could influence chlorophyll distribution.

Despite its relatively low resolution (7 km) in comparison with the bay's dimensions, our model was able to reproduce local changes in chlorophyll concentrations.

The annual chlorophyll signal near the coast (< 200 km) in this zone has been described as governed by wind stress and currents associated with westward-propagating Rossby waves (Correa-Ramírez et al., 2012). In the coastal transition zone (CTZ, west of the shelf break) increased chlorophyll concentrations are the result of nutrient advection by mesoscale eddies generated near the coast (Morales et al., 2012). Many eddies are generated in spring and summer, fertilizing offshore waters in winter (Correa-Ramírez et al., 2007). The mesoscale patterns of Fe limitation in summer, shown in Fig. 7a-d, suggest that these structures, generated near the shelf break, are rich in macronutrients like nitrate and silicate.

Comparison of modeled chlorophyll concentrations with *in situ* observations at Station 18 showed similar annual cycles, with high concentrations above 20 m depth in spring and summer (Fig. 4b,c). This concurs with the reports of Daneri et al. (2000) and Montero et al. (2007), where the highest chlorophyll concentrations were found between summer and the middle of autumn. Increased solar radiation is one of the main factors that trigger phytoplankton blooms in the upwelling system off central-southern Chile (Montero et al., 2007). Our results confirmed that light limitation is stronger than nutrient limitation for several months (Fig. 7). Improvements in light conditions in summer coincide with a shallower thermocline and the intensification of upwelling favorable winds in the zone (Sobarzo et al., 2007). In addition to the favorable light conditions in the system, the timing of upwelling and relaxing events is a crucial modulator of the high level of productivity in the upwelling ecosystem off central-southern Chile (Daneri et al., 2012). Relaxation of upwelling provides the required stability to produce phytoplankton blooms (Daneri et al., 2000).

The annual nitrate, phosphate, and silicate variability of the *in situ* observations at Station 18 was similar to that generated by the model (Fig. 5). The concentrations of these nutrients were high in spring-summer, coinciding with the period of winds favorable to upwelling (Sobarzo et al., 2007). High nutrient concentrations, together with low oxygen concentrations, high salinity, and low temperature, are typical of Equatorial Subsurface Waters (ESSW) (Atkinson et al., 2002; Silva et al., 2009), which are transported by the Peru-Chile Undercurrent (PCUC) along the continental shelf off Peru and Chile (Strub et al., 1998; Vergara et al., 2016). This water mass is transported to the surface in the upwelling season, fertilizing the eutrophic layer with new nutrients, allowing the existence of a highly productive ecosystem (Daneri et al., 2000; Quiñones et al., 2010).

The co-limitation of nutrients and silicate balance were only estimated for diatoms, since as noted above, diatoms were the most important contributor to total chlorophyll (~ 70%). As expected from the annual cycle of solar radiation (Sobarzo et al., 2007) in autumn and winter (April-August), light limitation extended from the very nearshore region (< 100 km) to approximately 200 km offshore (Fig. 7). Our results indicate that Fe was the offshore limiting nutrient in spring (September-November). Similar results have been reported offshore of the study region (34°S; 92°W), in the southeastern edge of the Southeast Pacific gyre (Bonnet et al., 2008). These authors found that Fe controlled photosynthetic efficiency and primary production. They reported that primary production in the southeast flank of the gyre at 92°W was co-limited by nitrogen and Fe, while in the center of the gyre nitrogen was the limiting nutrient. Blain et al. (2008) found high concentrations of Fe (1.2 nM at 30 m and 3.4 nM at 200 m; see Fig. 6) above the shelf break in the presence of low oxygen concentrations. These concentrations were roughly within the same order of magnitude as those in our simulations, but modeled Fe was much weaker at greater depth (Fig. 6), suggesting that the parameterization of Fe sources on the

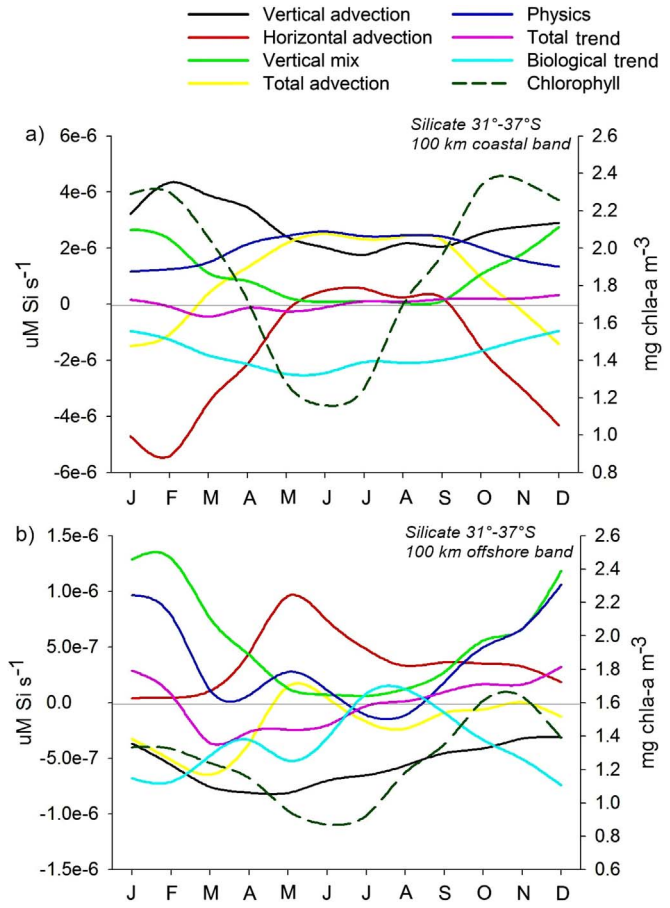

Fig. 11. Annual cycle of silicate transport terms within (a) a coastal band of 100 km, and (b) an offshore band of 100 km. Vertical advection (black), horizontal advection (red), total advection (yellow), vertical mixing (green), physical trend (blue), total trend (purple), biological trend (cyan). Surface chlorophyll (in mg Chl-a m^{-3}) is also shown (green dashed line). All fields are averaged between 0–20 m and 31° – 37°S.

shelf could be improved in the model. Thus, our estimation of Fe limitation near the coast remains uncertain and more measurements are needed for a more accurate evaluation of the model. Furthermore, the modeled MLD was too deep over most of the coastal domain and, particularly, in the northern part (30–34°S; Fig. 2) in winter (Fig. 2d). This suggests that light limitation may be overestimated and could play a less important role than that shown by the model during late fall-early winter (Fig. 7e-h).

There is evidence in the literature based on carbon and nutrient box model budgets (e.g. Gordon et al., 1996) that primary production may be limited by nitrogen in the northern and central-southern Chilean HCS (Quiñones et al., 2010). Lower N/P ratios relative to the Redfield N/P ratio in upwelling ecosystems have been associated with the presence of denitrification, which plays a key role in the nitrogen cycle in the OMZ (Farías et al., 2004, 2009b; Pantoja et al., 2004; Quiñones et al., 2010).

According to the results reported by Anabalón et al. (2016), for the same study zone, our findings on Si limitation are not far from reality. They found that macro-nutrient ratios (Si/N and N/P) experienced significant temporal changes which produced important modifications in the micro-phytoplankton community structure. Anabalón et al. (2016) reported a decrease in silicate and a moderate increase in nitrate produced by land-derived processes such as a reduction in river discharge, resulting in a large reduction (up to 100%) of the mean Si/N ratios. They emphasize that changes in Si/N ratio associated with increasing nitrate in coastal waters, without large changes in Si, influence diatom growth dynamics and eventually can lead to Si-limitation. They conclude that the dominance of different diatoms species in coastal waters may affect the ambient Si/N ratios through differences in their uptake rates.

Given that silicate was the main limiting nutrient in the simulations, the different terms of silicate transport were estimated to characterize their spatial and temporal variability. Despite its limited spatial resolution (7 km), the model was able to simulate preferential zones of vertical advection, i.e. enhanced coastal upwelling near 30–32°S, 33–34°S, 35–36°S and 37–38°S (Fig. 8a). Some of these areas are strong upwelling cells referred to in the literature: Punta Lengua de Vaca (30.24°S), Curaumilla (33.1°S), Punta Nugurne (35.9°S) and Punta Lavapie (37.15°S) (Aiken et al., 2008; Figueroa and Moffat, 2000; Strub et al., 1998). Punta Lavapie (37.15°S) has received special attention since is the most intense upwelling center of the Chilean HCS (Leth and Shaffer, 2001; Leth and Middleton, 2004; Valle-Levinson et al., 2003), and important for fishing productivity (Castillo et al., 1991; Cubillos et al., 2007; Landaeta and Castro, 2006). Greater spatial resolution is needed to better represent the dynamics of this particular region.

As expected, based on the conservation of mass balance, horizontal advection (Fig. 8d) partly balanced vertical advection. Interestingly, while coastal upwelling, and hence vertical advection was strongest in summer (Fig. 11a, black line), nutrient decrease due to horizontal advection was strong, thus the coastal region lost nutrients through advective processes. This loss was compensated by the entrainment of nutrients into the surface layer through vertical mixing (green line, Fig. 11a). Furthermore, enhanced eddy activity (related to horizontal process) tends to be associated with low levels of biological production, exerting a suppressive effect on upwelling systems (Gruber et al., 2011).

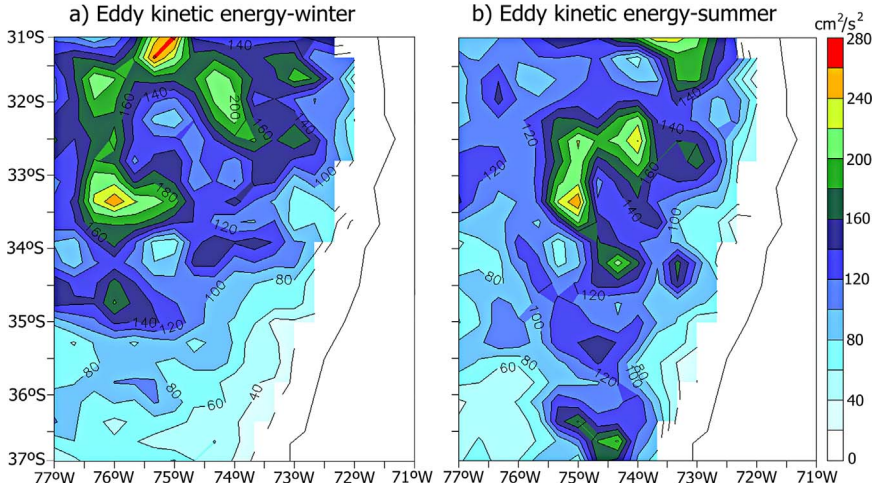

Fig. 12. Surface Eddy Kinetic Energy (in $cm^2\ s^{-2}$) during winter (a) and summer (b).

Our simulations show that in contrast to the coastal zone, offshore vertical advection was negative, with greater values in spring-summer, suggesting year-round downwelling. Using a regional physical model, Aguirre et al. (2012) described the importance of offshore upwelling/downwelling linked to Ekman pumping. They found a region offshore with anticyclonic curl associated with downwelling forced by Ekman suction. Thus, it is probable that the vertical advection offshore in our simulations is linked to Ekman suction. The latter was offset by horizontal advection, which fueled the region in autumn-winter (from April to September, Fig. 11b). These results may be related to eddy-induced nutrient transport from the nearshore environment to the open ocean (Correa-Ramirez et al., 2007).

The present model approach has some limitations. Monthly climatological winds and boundary conditions used to force the model allowed for representing the seasonal variability of the system with a fair degree of realism. Nevertheless, intraseasonal wind variability (*e.g.*, Gomez et al., 2017) and coastal trapped waves (Hormazábal et al., 2002) can modulate nearshore primary production, as occurs in the Peru EBUS (*e.g.,* Echevin et al., 2014). These fluctuations were not well represented as the climatological boundary forcing smoothed the dominant 60-day variability. Furthermore, strong episodic upwelling events that typically last one to two weeks (Leth and Middleton, 2004; Sobarzo et al., 2007) were not represented in the climatological wind forcing. Investigating the impact of physical processes not accounted for in this study on the biogeochemical ecosystem will be addressed in future work.

5. Conclusions

For the first time, an eddy-resolving three-dimensional ocean circulation model coupled to an intermediate-complexity biogeochemical model simulated the spatial and seasonal variability of nutrients and chlorophyll in the HCS off central-southern Chile (30–40°S). The annual cycles of modeled nutrients (nitrate, silicate, and phosphate) were similar to cycles observed at a coastal station (Station 18) and to satellite observations (SeaWIFS), with the highest values in spring and summer, in agreement with upwelling observations. Although modeled chlorophyll showed a spatial pattern and annual cycle similar to those of the SeaWIFS satellite data, the modeled concentrations did not exceed 4 mg Chl-a m^{-3} along the coast, while the maximum observed concentration by SeaWIFS was 10 mg m^{-3}. The modeled annual chlorophyll cycle was also similar to the cycle at Station 18, with the highest values in spring and summer in the first 20 m of the water column. However, simulated concentrations did not exceed 3.5 mg m^{-3}, while those at Station 18 reached up to 12 mg m^{-3}. The spatial distribution of the modeled mixed layer was similar to a low-resolution (2°) climatology, with lower values near the coast and higher values offshore, although the modeled mixed layer was deeper in winter than the observed mixed layer depth.

Co-limitation of phytoplankton growth by light and several nutrients was investigated using the model. Near the coast, photosynthesis was mainly governed by light during autumn and winter, and by silicate during the rest of the year. Offshore co-limitation was mainly due to nitrate in summer and autumn, and Fe during winter and spring. Occasionally Fe, nitrate and phosphate were also limiting within and around mesoscale eddies, revealing complex structures.

The spatial structure and seasonality of silicate fluxes in the surface layer (0–20 m) were characterized. Vertical advection highlighted positive areas nearshore associated with greater coastal upwelling and negative areas offshore due to Ekman suction. The strong upward flux exerted by coastal upwelling was fully offset by horizontal fluxes resulting in negative total advective flux in summer. Enhanced horizontal advection could be related to eddy-induced transport of nutrients from the nearshore region to the open ocean during the upwelling period. Upward nutrient flux through vertical mixing played a major role throughout the year, particularly in summer. This study constitutes a first step to modeling the seasonal cycle of three-dimensional coupled physical-biogeochemical processes in central-southern Chile.

Acknowledgements

This study was funded by the Interdisciplinary Center for Aquaculture Research (INCAR; FONDAP Project N°15110027; CONICYT) and by the Programa de Investigación Marina de Excelencia (PIMEX) of the Faculty of Natural and Oceanographic Sciences (University of Concepción, Chile) funded by Celulosa Arauco y Constitución S.A.(Grant N° NP-4503534245) Odette Vergara was also supported by a Doctoral Scholarship from the Comisión Nacional de Investigación Científica y Tecnológica (CONICYT, Ministry of Education, Chile). We acknowledge the financial support for O. Vergara's internships at LOCEAN received from the French Embassy in Chile and the REDOC-CTA (Grant Number UCO-1202; Red Doctoral en Ciencia, Tecnología y Ambiente, University of Concepción, Chile).

References

Aguirre, C., Pizarro, O., Strub, P.T., Garreaud, R., Barth, J., 2012. Seasonal dynamics of the near-surface alongshore flow off central Chile. J. Geophys. Res. 117, 1–17.
Aiken, C., Castillo, M., Navarrete, S., 2008. A simulation of the Chilean Coastal Current and associated topographic upwelling near Valparaíso, Chile. Cont. Shelf Res. 28 (17), 2371–2381.
Anabalón, V., Morales, C.E., González, H.E., Menschel, E., Schneider, W., Hormazábal, S., Valencia, L., Escribano, R., 2016. Micro-phytoplankton community structure in the coastal upwelling zone off Concepción (central Chile): annual and inter-annual fluctuations in a highly dynamic environment. Prog. Oceanogr. 149, 174–188.
Atkinson, L.P., Valle-Levinson, A., Figueroa, D., De Pol-Holz, R., Gallardo, V.A., Schneider, W., Blanco, J.L., Schmidt, M., 2002. Oceanographic observations in Chilean coastal waters between valdivia and concepción. J. Geophys. Res. 100, 181–193.
Aumont, O., Maier-Reimer, E., Blain, S., Monfray, P., 2003. An ecosystem model of the global ocean including Fe, Si, P colimitations. Glob. Biogeochem. Cycles 17 (2), 1060.
Aumont, O., Bopp, L., 2006. Globalizing results from ocean in situ iron fertilization studies. Glob. Biogeochem. Cycles 20http://dx.doi.org/10.1029/2005GB002591. (GB2017).
Aumont, O., Ethé, C., Tagliabue, A., Bopp, L., Gehlen, M., 2015. PISCES-v2: an ocean biogeochemical model for carbon and ecosystem studies. Geosci. Model Dev. Discuss. 8, 1375–1509.
Baird, M.E., Leth, O., Middleton, J.F., 2007. Biological response to circulation driven by mean summertime winds off central Chile: a numerical model study. J. Geophys. Res. 112, C07031. http://dx.doi.org/10.1029/2006JC003655.
Bakun, A., 1996. Patterns in the Ocean. Ocean Processes and Marine Population Dynamics. California Sea Grant Colllege System, USA, in cooperation with Centro de Investigaciones Biológicas del Norte, La Paz, Baja California Sur, pp. 323.
Bakun, A., Nelson, C.S., 1991. The seasonal cycle of wind-stress curl in subtropical eastern boundary current regions. J. Phys. Oceanogr. 21, 1815–1834.
Blain, S., Bonnet, S., Guieu, C., 2008. Dissolved iron distribution in the tropical and sub tropical South Eastern Pacific. Biogeoscience 5, 269–280.
Bonnet, S., Guieu, C., Bruyant, F., Prásil, O., Van Wanbeke, F., Raimbault, P., Moutin, T., Grob, C., Gorbunov, M.Y., Zehr, J.P., Masquelier, S.M., Garzarek, L., Claustre, H., 2008. Nutrient limitation of primary productivity in the Southeast Pacific (BIOSOPE cruise). Biogoscience 5, 215–225.
Blumberg, A.F., Mellor, G.L., 1987. A description of a three- dimensional coastal ocean circulation model. In: In: Heaps, N. (Ed.), Three-Dimensional Coastal Ocean Models 4. AGU, Washington, D.C., pp. 1–16 Coastal Estuarine Series.
Brochier, T., Echevin, V., Tam, J., Chaigneau, A., Goubanova, K., Bertrand, A., 2013. Climate change scenarios experiments predict a future reduction in small pelagic fish recruitment in the Humboldt current system. Glob. Change Biol. 19, 1841–1853.
Bruland, K.W., Rue, E.L., Smith, G.J., DiTullio, G.R., 2005. Iron, macronutrients and diatom blooms in the Peru upwelling regime: brown and blue waters of Peru. Mar. Chem. 93, 81–103.
Castillo, G., Muñoz, H., González, H., Bernal, P., 1991. Daily analysis of abundance and size variability of fish larvae in relation to oceanic water intrusions in coastal areas. Biol. Pesq. 20, 21–35.
Chávez, F.P., Ryan, J., Lluch-Cota, S.E., Ñiquen, M., 2003. From Anchovies to sardines and back: multidecadal change in the Pacific Ocean. Science 299 (5604), 217–221.
Chávez, F.P., Messié, M., 2009. A comparison of eastern boundary upwelling ecosystems, Progr. Oceanogr 83 (1–4), 80–96.
Colas, F., McWilliams, J.C., Capet, X., Kurian, J., 2012. Heat balance and eddies in the Peru-Chile current system. Clim. Dyn. 39 (1–2), 509–529.
Correa-Ramirez, M.A., Hormazábal, S., Yuras, G., 2007. Mesoscale eddies and high chlorophyll concentrations of central Chile (29–39°S). Geophys. Res. Lett. 34 (12). http://dx.doi.org/10.1029/2007GL029541.
Correa-Ramirez, M.A., Hormazábal, S., Morales, C.E., 2012. Spatial patterns of annual and interannual surface chlorophyll-a variability in the Peru-Chile current system. Prog. Oceanogr. 92–95, 8–17.
Cubillos, L.A., Ruiz, P., Claramunt, G., Gacitúa, S., Nuñez, S., Castro, L., Riquelme, K.,

Alarcón, C., Oyarzún, C., Sepúlveda, A., 2007. Spawning, daily egg production, and spawning stock biomass estimationfor common sardine (Strangomera bentincki) and anchovy (Engraulis ringens) off central southern Chile in 2002. Fish. Res. 86, 228–240.
Daneri, G., Dellarossa, V., Quiñones, R., Jacob, B., Montero, P., Ulloa, O., 2000. Primary production and community respiration in the Humboldt Current System off Chile and associated oceanic areas. Mar. Ecol. Progr. Ser. 197, 41–49.
Daneri, G., Lizárraga, L., Montero, P., González, H.E., Tapia, F.J., 2012. Wind forcing and short-term variability of phytoplankton and heterotrophic bacterioplankton in the coastal zone of the Concepción upwelling system (central Chile). Prog. Oceanogr. 92–95, 92–96.
Da Silva, A.M., Young, C.C., Levitus, S. (Eds.), 1994. Atlas of Surface Marine Data 1994, vol. 1. Algorithms and Procedures. NOAA Atlas NESDIS, vol. 6. U. S., NOAA, Silver Spring, MD, pp. 83 Technical Report.
de Boyer Montégut, C., Madec, G., Fischer, A.S., Lazar, A., Iudicone, D., 2004. Mixed layer depth over the global ocean: an examination of profile data and a profile-based climatology. J. Geophys. Res. 109, C12003. http://dx.doi.org/10.1029/2004JC002378.
Diehl, S., Berger, S., Ptacnik, R., Wild, A., 2002. Phytoplankton, light, and nutrients in a gradient of mixing depths: field experiments. Ecology 83, 399–411.
Echevin, V., Aumont, A., Ledesma, J.M., Flores, G., 2008. The seasonal cycle of surface chlorophyll in the Peruvian upwelling System: a modeling Study. Progress. Oceanogr. 79, 167–176.
Echevin, V., Albert, A., Lévy, A., Graco, M., Aumont, O., Piétri, A., Garric, G., 2014. Intraseasonal variability of nearshore productivity in the Northern Humboldt Current System: the role of coastal trapped waves. Cont. Shelf Res. 73, 14–30.
Eppley, R.W., Peterson, B.J., 1979. Particulate organic matter flux and planktonic new production in the deep ocean. Nature 282, 677–680.
Escribano, R., Schneider, W., 2007. The structure and functioning of the coastal upwelling system off central/southern Chile. Progress. Oceanogr. 75, 343–347.
Falkowski, P.G., Barber, R.T., Smetacek, V., 1998. Biogeochemical controls and feedbacks on ocean primary production. Science 281, 200–206.
Farías, L., Graco, M., Ulloa, O., 2004. Nitrogen cycling in continental shelf sediments of the upwelling ecosystem off central Chile. Deep Sea Res. Part II 51, 2491–2505.
Farías, L., Castro-González, M., Cornejo, M., Charpentier, J., Faúndez, J., Boontanon, N., Yoshida, N., 2009b. Denitrification and nitrous oxide cycling within the upper oxycline of the eastern tropical South Pacific oxygen minimum zone. Limnol. Oceanogr. 1 (54), 132–144.
Figueroa, A.D., Moffat, C., 2000. On the influence of topography in the induction of coastal upwelling along the Chilean coast. Geophys. Res. Lett. 27, 3905–3908.
Giraud, X., Le Quéré, C., da Cunha, L.C., 2008. Importance of coastal nutrient supply for global ocean biogeochemistry. Glob. Biogeochem. Cycles 22, GB2025. http://dx.doi.org/10.1029/2006GB002717.
Gomez, F.A., Spitz, Y.H., Batchelder, H.P., Correa-Ramirez, M.A., 2017. Intraseasonal patterns in coastal plankton biomass off central Chile derived from satellite observations and a biochemical model. J. Mar. Syst. http://dx.doi.org/10.1016/j.jmarsys.2017.05.003.
Gordon D.C. Jr, Boudreau P.R., Mann K.H., 1996. LOICZ Biogeochemical Modelling Guidelines. LOICZ Reports & Studies No 5.
Gruber, N., Lachkar, Z., Frenzel, H., Marchesiello, P., Munnich, M., McWilliams, J.C., Nagai, T., Plattner, G.-K., 2011. Eddy-induced reduction of biological production in eastern boundary current system. Nat. Geosci. 4, 787–792.
Grob, C., Quiñones, R.A., Figueroa, D., 2003. Quantification of coast-ocean water transport through filaments and eddies with high chlorophyll-a content, in central-south Chile (35.5–37.5°S). Gayana 67, 55–67.
Hill, A.E., Hickey, B.M., Shillington, F.A., Strub, P.T., Brink, K.H., Barton, E.D., Thomas, A.C., 1998. Eastern Ocean boundaries. In: Robinson, A.R., Brink, K.H. (Eds.), The Sea 11. John Wiley, Hoboken, N. J, pp. 29–67.
Hernández, K., Yannicelli, B., Montecinos, A., Ramos, M., González, H.E., Daneri, G., 2012. Temporal variability of incidental solar radiation and modulating factors in a coastal upwelling area (36°S). Progress. Oceanogr. 92 (1), 18–32.
Hormazábal, S., Shaffer, G., Pizarro, O., 2002. Tropical Pacific control of intraseasonal oscillations off Chile by way of oceanic and atmospheric pathways. Geophys. Res. Lett. 29, 6.
Hutchins, D.A., Bruland, K.W., 1998. Fe-limited diatom growth and Si:N uptake ratios in a coastal upwelling regime. Nature 393, 561–564.
Hutchins, D.A., DiTullio, G.R., Zhang, Y., Bruland, K.W., 1998. An iron limitation mosaic in the California upwelling regime. Limnol. Oceanogr. 43, 1037–1054.
Hutchins, D.A., Hare, C.E., Weaber, R.S., Zhang, Y., Fire, G.F., DiTullio, G.R., Alm, M.B., Riseman, S.F., Maucher, J.M., Geesey, M.D., Trick, C.G., Smith, G.J., Rue, E.L., Conn, J., Bruland, K.W., 2002. Phytoplankton iron limitation in the Humboldt current and Peru upwelling. Limnol. Oceanogr. 47 (4), 997–1011.
Huyer, A., Knoll, M., Paluszkiewicz, T., Smith, R., 1991. The Perú undercurrent: a study in variability. Deep Sea Res. 38, 247–279.
Iriarte, J.L., Vargas, C., Tapia, F.J., Bermúdez, R., Urrutia, R.E., 2012. Primary production and plankton carbon biomass in a river-influenced upwelling area off Concepción, Chile. Progress. Oceanogr. 92 (1), 97–109.
José, Y.S., Aumont, O., Machu, E., Penven, P., Moloney, C.L., Maury, O., 2014. Influence of mesoscale eddies on biological production in the Mozambique Channel: several contrasted examples from a coupled ocean-biogeochemistry model. Deep Sea Res. II 100, 79–93.
Kara, A.B., Rochford, P.A., Hurlburt, H.E., 2003. Mixed layer depth variability over the global ocean. J. Geophys. Res. 108 (C3), 3079. http://dx.doi.org/10.1029/2000JC000736.
Kirk, J.T.O., 1994. Light and Photosynthesis in Aquatic Ecosystems, Second ed. Cambridge University Press, Cambridge, United Kingdom, pp. 509.
Kuypers, M.M.M., Lavik, G., Woebken, D., Schmid, M., Fuchs, B.M., Amman, R., Jorgensen, B.B., Jetten, M.S.M., 2005. Massive nitrogen loss from the Benguela upwelling system through anaerobic ammonium oxidation. PNAS 108, 6478–6483.
Lachkar, Z., Gruber, N., 2011. What controls biological production in coastal upwelling systems? Insights from a comparative modeling study. Biogeosciences 8, 2961–2976.
Landaeta, M.F., Castro, L.R., 2006. Spawning and larval survival of the Chilean hake Merluccius gayi under later summer conditions in the Gulf of Arauco, central Chile. Fish. Res. 77, 115–121.
Large, W.G., MacWilliams, J.C., Doney, S.C., 1994. Oceanic vertical mixing a review and a model with a nonlocal boundary layer parameterization. Rev. Geophys. 32, 363–403.
Leth, O., Shaffer, G., 2001. A numerical study of the seasonal variability in the circulation off central Chile. J. Geophys. Res. 106 (C10), 229–248.
Leth, O., Middleton, J.F., 2004. A mechanism for enhanced upwelling off central Chile: eddy advection. J. Geophys. Res. 109 (C12020), 1–17.
Lorbacher, K., Dommenget, D., Niiler, P.P., Kohl, A., 2006. Ocean mixed layer depth: a subsurface proxy of ocean-atmosphere variability. J. Geophys. Res. 111, C07010. http://dx.doi.org/10.1029/2003JC002157.
Marín, V., Delgado, L., Escribano, R., 2003. Upwelling shadows at Mejillones Bay (northern Chilean coast): a remote sensing in situ analysis. Invest. Mar. Valparaíso 31 (2), 47–55.
Mason, E., Molemaker, J., Shchepetkin, A.F., Colas, F., McWilliams, J.C., Sangrá, P., 2010. Procedures for offline grid nesting in regional ocean models. Ocean Model. 35, 1–15.
Mesias, J., Matano, R., Strub, P.T., 2001. A numerical study of the upwelling circulation off central Chile. J. Geophys. Res. 106, 611–623.
Messié, M., Chávez, F., 2015. Seasonal regulation of primary production in eastern boundary upwelling systems. Prog. Oceanogr. 134, 1–18.
Montero, P., Daneri, G., Cuevas, A., González, H., Jacob, J., Lizárraga, L., Menschel, E., 2007. Productivity cycles in the upwelling area off concepción: the importance of diatoms and bacterioplankton in the organic carbon flux. Prog. Oceanogr. 75, 518–530.
Moore, J.K., Doney, S.C., Lindsay, K., 2004. Upper ocean ecosystem dynamics and iron cycling in a global three-dimensional model. Glob. Biogeochem. Cy. 18, GB4028. http://dx.doi.org/10.1029/2004GB002220.
Moore, C.M., Mills, M.M., Arrigo, K.R., Berman-Frank, I., Bopp, L., Boyd, P.W., Galbraith, E.D., Geider, R.J., Guieu, C., Jaccard, S.L., Jickells, T.D., La Roche, J., Lenton, M., Mahowald, N.M., Marañón, E., Marinov, I., Moore, J.K., Nakatsuka, T., Oschlies, A., Saito, M.A., Thingstad, T.F., Tsuda, A., Ulloa, O., 2013. Processes and patterns of oceanic nutrient limitation. Nat. Geosci. 6, 701–710.
Morales, C.E., Hormazábal, S., Correa-Ramírez, M., Pizarro, O., Silva, N., Fernández, C., Anabalón, V., Torreblanca, M.L., 2012. Mesoscale variability and nutrient–phytoplankton distributions off central-southern Chile during the upwelling season: the influence of mesoscale eddies. Prog. Oceanogr. 104, 17–29.
Morales, C.E., Hormazábal, S., Andrade, I., Correa-Ramírez, M., 2013. Time-space variability of chlorophyll-a and associated physical variables within the region off central-Southern Chile. Remote Sens. 5, 5550–5571.
Nicklisch, A., Shatwell, T., Kohler, J., 2008. Analysis and modelling of the interactive effects of temperature and light on phytoplankton growth and relevance for the spring bloom. J. Plankton Res. 30 (1), 75–91.
Pantoja, S., Sepulveda, J., Gonzalez, H.E., 2004. Decomposition of sinking proteinaceous material during fall in oxygen minimum zone off northern Chile. Deep-Sea Res. I 51, 55–70.
Penven, P., Debreu, L., Marchesiello, P., McWilliams, J.C., 2006. Evaluation and application of the ROMS 1-way embedding procedure to the central california upwelling system. Ocean Model. 12, 157–187.
Peterson, D.H., Perry, M.J., Bencala, K.E., Talbot, M.C., 1987. Phytoplankton productivity in relation to Light Intensity: a simple equation. Estuar. Coast. Shelf Sci. 24, 813–832.
Pickard, G.L., Emery, W.J., 1990. Descriptive Physical Oceanography. Pergamon, Tarrytown, N.Y, pp. 320.
Quiñones, R.A., Gutiérrez, M.H., Daneri, G., Gutiérrez, D.A., González, H.E., Chávez, F., 2010. Pelagic carbon fluxes in the Humboldt Current System. In: Liu, K.K., Atkinson, L., Quiñones, R.A., Talaue-McManus, L. (Eds.), Carbon and Nutrient Fluxes in Global Continental Margins: a Global Synthesis. Springer-Verlag, New York, NY, pp. 44–64.
Resplandy, L., Lévy, M., Madec, G., Pous, S., Aumont, O., Kumar, D., 2011. Contribution of mesoscale processes to nutrient budgets in the Arabian Sea. J. Geophys. Res. 116, C11007. http://dx.doi.org/10.1029/2011JC007006.
Ridgway, K.R., Dunn, J.R., Wilkin, J.L., 2002. Ocean interpolation by four-dimensional least squares applications to the waters around Australia. J. Atmos. Ocean Technol. 19 (9), 1357–1375.
Salamanca, M., Pantoja, S., 2009. Caracterización química de la zona marina adyacente a la desembocadura del río Itata. La Cuenca del Río Itata: La cuenca hidrográfica del Itata: Aportes científicos para su gestión sustentable, pp. 177-191. Parra, O. Castilla J. C., Quiñones, H.R.A., Camaño, A (Eds.). Ediciones Universidad de Concepción, Concepción, Chile. 389 pp.
Silva, N., Neshyba, S., 1979. On the southernmost extension of the Perú-Chile Undercurrent. Deep Sea Res. 26, 1387–1393.
Sobarzo, M., Figueroa, D., Djurfeldt, L., 2001. Upwelling of subsurface water into the rim of the Biobio submarine canyon as a response to surface wind. Cont. Shelf Res. 21, 279–299.
Sobarzo, M., Saldías, G.S., Tapia, F.J., Bravo, L., Moffat, C., Largier, J.L., 2016. On subsurface cooling associated with the Biobio river Canyon (Chile). J. Geophys. Res. Oceans 121, 4568–4584.
Sobarzo, M., Bravo, L., Donoso, D., Garcés-Vargas, J., Schneider, W., 2007. Coastal upwelling and seasonal cycles that influences the water column over the continental shelf of central Chile. Progr. Oceanogr. 75, 363–382.
Strub, P.T., Mesías, J., Montecino, V., Ruttlant, J., Salinas, S., 1998. Coastal ocean circulation off Western South America. Coastal Segment (6, E). In: Robinson, A., Brink,

K. (Eds.), The Sea 11. John Wiley & Sons, Hoboken, pp. 273–313.
Strub, P.T., Mesias, M., James, C., 1995. Altimeter observations of the Perú-Chile Countercurrent. Geophys. Res. Lett. 22, 211–214.
Silva, N., Rojas, N., Fedele, A., 2009. Water masses in the Humboldt Current System: properties, distribution, and the nitrate deficit as a chemical water mass tracer for equatorial subsurface water off Chile. Deep-Sea Res. Ii. 56, 1004–1020.
Schepetkin, A., McWilliams, J.C., 2005. The regional oceanic modeling system (ROMS): a split-explicit, free-surface, topography-following- coordinate oceanic model. Ocean Model. 9, 347–404.
Sverdrup, H.U., 1953. On conditions for the vernal blooming of phytoplankton. J. Cons. Int. Explor. Mer. 18, 287–295.
Tegen, I., Fung, I., 1995. Contribution to the atmospheric mineral aerosol load from land surface modification. J. Geophys. Res. 100 (D9), 18707–18726. http://dx.doi.org/10.1029/95JD02051.
Thomas, M.K., Kremer, C.T., Klausmeier, C.A., Litchamn, E., 2012. A global pattern of thermal adaptation in marine phytoplankton. Science 338 (6110), 1085–1088. http://dx.doi.org/10.1126/science.1224836.
Valle-Levinson, A., Atkinson, L.P., Figueroa, D., Castro, L., 2003. Flow induced by upwelling winds in an equatorward facing bay: gulf of Arauco, Chile. J. Geophys. Res. 108 (3054). http://dx.doi.org/10.1029/2001JC001272. (C2).
Vargas, C., Contreras, P.Y., Iriarte, J.L., 2012. Relative importance of phototrophic, heterotrophic, and mixotrophic nanoflagellates in the microbial food web of a river-influenced coastal upwelling area. Aquat. Microb. Ecol. 65, 233–248.
Vergara, O.A., Echevín, V., Sepúlveda, H.H., Colas, F., 2016. Modelling the seasonal dynamics of the Peru-Chile Undercurrent off Central Chile (30–40°S). Cont. Shelf. Res. 123, 61–79.
Wijesekera, R.W., Gregg, M.C., 1996. Surface layer response to weak winds, westerly bursts, and rain squalls in the western Pacific warm pool. J. Geophys. Res. 101, 977–997.
Zehr, J.P., Ward, B.B., 2002. Nitrogen cycling in the Ocean: new perspectives on processes and paradigms. Appl. Environ. Microbiol. 68 (3), 1015–1024.